Numerical validation of an Homogenized Interface Model

Giuseppe Geymonat, Sofiane Hendili, Françoise Krasucki, Marina Vidrascu

Numerical validation of an Homogenized Interface Model[☆]

Giuseppe Geymonat[a], Sofiane Hendili[b], Françoise Krasucki[c], Marina Vidrascu[d,e]

[a] *LMS, UMR-CNRS 7649, Ecole Polytechnique,Route de Saclay 91128 Palaiseau Cedex*
[b] *CEA, DEN, DANS, DM2S, SEMT, Laboratoire de Modélisation et de Simulation des Structures, 91191 Gif-sur-Yvette, France*
[c] *I3M, UMR-CNRS 5149, Université Montpellier 2, Case courier 051, Place Eugène Bataillon, 34095 Montpellier Cedex 5*
[d] *Inria, REO project-team, Rocquencourt - B.P. 105, F–78153 Le Chesnay cedex, France*
[e] *UPMC Univ Paris VI, REO project-team, UMR 7958 LJLL, F–75005 Paris, France*

Abstract

Our aim is to validate the effectiveness of a matched asymptotic expansion method introduced in [1], [2]. A simplified model for the influence of small identical heterogeneities periodically distributed on an internal surface is obtained and applied to the overall response of a linearly elastic body. A careful numerical study compares the solution obtained by a standard method on a fine mesh to the one obtained by asymptotic expansion. We compute both the zero th and first order terms in the expansion. To efficiently compute the first order term we introduce a domain decomposition method.

Keywords: finite element method, linear elasticity, matched asymptotic expansions, domain decomposition

[☆]This work was partially supported by the French Agence Nationale de la Recherche (ANR) under Grant Epsilon (BLAN08-2 312370) (Domain decomposition and multi-scale computations of singularities in mechanical structures); it is a natural continuation of the Thesis of Sofiane Hendili carried out at I3M and INRIA and supported by Grant Epsilon.

Email addresses: `giuseppe.geymonat@lms.polytechnique.fr` (Giuseppe Geymonat), `s_hendili@yahoo.fr` (Sofiane Hendili), `krasucki@math.univ-montp2.fr` (Françoise Krasucki), `marina.vidrascu@inria.fr` (Marina Vidrascu)

Contents

1 Introduction **2**

2 Asymptotic model **4**
2.1 The problem 4
2.2 The inner-outer matched asymptotic method 6
2.2.1 Theoretical results for the asymptotic study 10
2.3 Definition of the outer and inner approximations 15

3 Solution of the first order problem by domain decomposition **15**
3.1 A linear elasticity model problem 15
3.2 Solution of the first order problem 17
3.3 Implementation issues 19

4 Validation **20**
4.1 Description of the test problem 21
4.2 Numerical solution of the cell problems 22
4.2.1 Dependence on L^∞ 23
4.2.2 Dependence on f 24
4.2.3 Dependence on R 25
4.2.4 Dependence on E^I/E in the case of elastic inclusions with $p = 0$ 27
4.3 Validation at the macroscopic scale 27
4.4 Validation at the microscopic scale 34

5 Concluding remarks **38**

1. Introduction

For various research applications in fields spanning the mathematical, physical and engineering communities, there is great interest in a rigorous and efficient numerical approximation of the solution of boundary value problems where the domain and/or the coefficients have a large number of heterogeneities When the characteristic size of the heterogeneitis is much smaller than the whole structure and the heterogeneities are periodically distibuted in all the volume a now classical approach is to use an homogenization method [3], [4], [5], [6]. Simplified models for multi-materials consider two elastic bodies connected by a strong thin material layer whose stiffness grows [7],

[8] or by a thin adhesive layer [9]. The situation is different when the heterogeneities are periodically distributed on an internal surface ω. In this case an alternative approach is mandatory. The analysis of the behaviour of a structure made of a material with a large number of heterogeneities distributed on a surface using a standard finite element method becomes very expensive when the characteristic size of the heterogeneity is much smaller than the whole structure. In this case an alternative approach is to use a multi-scale method such as those proposed in [10], [11] in the framework of matched asymptotic expansions and more recently developed in [12], [13], [14], [15]. The first objective of this paper is to numerically validate a recently proposed new method [1], [2] and the second one is to introduce a numerical algorithm which accurately implements the method. Basically the matched asymptotic expansions allow to replace the initial problem by a set of new ones: the layer of heterogeneities is replaced by a surface (in 3D) or a line in (2D) on which particular jumping conditions are defined. These are the macroscopic problems. The definition of these problems requires several quantities which are computed via the solution of cell problems at the microscopic level. The paper is organized as follows: in Section 2 we set the problem and briefly recall the asymptotic analysis of this problem based on the matched asymptotic expansion method. Specifically we assume that the displacement and stress fields admit two asymptotic expansions, one far from the heterogeneities (the outer one) another one close (the inner one). The construction of the outer and inner problem allows to define the transmission coefficients across the surface. We show that the order 0 outer problem is independent of the heterogeneities. For the first order outer problem the transmission coefficients are given by several elementary inner problems posed on a representative cell. These problems depend on the nature of the heterogeneities (holes, highly contrasted materials). In Section 3 we introduce a domain decomposition type algorithm to numerically solve the first order problem (the problem with jumps on an internal boundary). Finally in Section 4 we validate the whole procedure by comparing, on a test problem, the solution obtained using standard finite elements on a large mesh to the solution obtained by the asymptotic approach.

2. Asymptotic model

2.1. The problem

Let us consider a three dimensional structure Ω (an open domain of $\mathbb{R}^3$ with smooth boundary $\partial\Omega$) containing small identical heterogeneities periodically distributed along a surface ω that we assume for simplicity contained in the plane $x_1 = 0$ (see Fig. 1). We assume that ω is contained in the union of

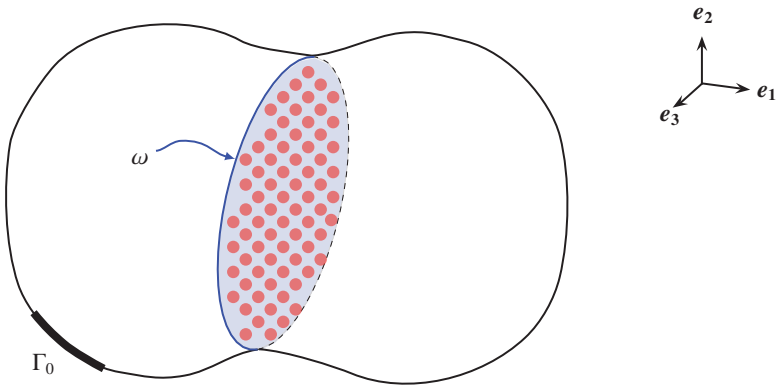

Figure 1: The structure with the layer of heterogeneities

$\mathcal{N}(\varepsilon) \approx \dfrac{aire(\omega)}{aire(\hat{Y})}\varepsilon^{-2}$ sets $\varepsilon\hat{Y}$, where $\hat{Y} \subset \mathbb{R}^2$ is the basis of a periodic planar net (we take for simplicity $\hat{Y} =]-\frac{1}{2},\frac{1}{2}[\times]-\frac{1}{2},\frac{1}{2}[$). Let I be a non-empty $3D$ domain contained in $\mathbb{R}\times\hat{Y}$ with smooth boundary ∂I, with diameter d satisfying $0 < \dfrac{d}{diam(\Omega)} < +\infty$ and such that $I \cap \{x_1 = 0\}$ is strictly contained in $\hat{Y}$ (hence $d < \sqrt{2}$). We also assume that the heterogeneities have a diameter εd and fill every domain εI. We denote by $\varepsilon\partial I$ the boundary of εI and by $\mathcal{I}^\varepsilon$, resp. $\partial\mathcal{I}^\varepsilon$, the union of all the heterogeneities, resp. of all their boundaries.

Hence from a geometrical point of view there are two natural length scales: the first is a global one (the $3D$-diameter of Ω or the $2D$-diameter of ω) the other one is a local one connected with the heterogeneities (e.g. the diameter of each heterogeneity). The ratio between these two scales will be denoted by ε. More precisely, the parameter ε is a non-dimensional parameter characterizing the geometrical distribution of the heterogeneities in the structure

since, at the same time, it characterizes the ratio between the diameter of any heterogeneity (εd) and the diameter of Ω and the ratio between the diameter of the period ($\varepsilon \hat{Y}$) of the planar net and the diameter of the planar set ω supporting the heterogeneities.

In this work we consider two types of inclusions: holes and soft elastic inclusions with stiffness dependent on ε. In the case of elastic inclusions, transmission conditions must be verified on $\partial\mathcal{I}^\varepsilon$, while free boundary conditions must be taken into account on $\partial\mathcal{I}^\varepsilon$ in the case of the holes. The boundary of Ω is composed of two parts Γ_0 and Γ_F with $\partial\Omega = \overline{\Gamma_0} \cup \overline{\Gamma_F}$ and $\Gamma_0 \cap \Gamma_F = \emptyset$. The structure is clamped on Γ_0 and a density $\boldsymbol{F}$ of surface forces is applied on the complementary part Γ_F. Let $\boldsymbol{u}^\varepsilon$ and $\boldsymbol{\sigma}^\varepsilon$ be the displacement and the stress field at equilibrium. These fields verify the following equations:

$$\begin{cases} \boldsymbol{div}\boldsymbol{\sigma}^\varepsilon = \boldsymbol{0} & \text{in } \Omega^\varepsilon \\ \boldsymbol{\sigma}^\varepsilon = \boldsymbol{A}\boldsymbol{\gamma}(\boldsymbol{u}^\varepsilon) & \text{in } \Omega^\varepsilon \\ \boldsymbol{\sigma}^\varepsilon \boldsymbol{n} = \boldsymbol{F} & \text{on } \Gamma_F \\ \boldsymbol{u}^\varepsilon = \boldsymbol{0} & \text{on } \Gamma_0 \end{cases} \tag{1}$$

where

- $$\Omega^\varepsilon = \begin{cases} \Omega \backslash \mathcal{I}^\varepsilon & \text{in the holes case} \\ \Omega & \text{in the elastic inclusions case} \end{cases}$$
- $$\boldsymbol{A} = \begin{cases} \boldsymbol{A}^S & \text{in } \Omega \backslash \mathcal{I}^\varepsilon \\ \varepsilon^p \boldsymbol{A}^I \ , \ p \in \mathbb{N} & \text{in } \mathcal{I}^\varepsilon \text{ (in the case of elastic inclusions)} \end{cases} \tag{2}$$

  with A^S and A^I of same order.

Let us stress that in the case of elastic inclusions as shown in (2) the parameter ε is a non-dimensional parameter characterizing at the same time the geometrical distribution of the heterogeneities in the structure and the ratio between the rigidity of the heterogeneities and the rigidity of the structure.

The inner-outer matched asymptotic method approximates the initial problem with a set of new ones defined in Ω where the layer of heterogeneities is replaced by the surface ω (see Fig. 2) where suitable transmission conditions are defined.

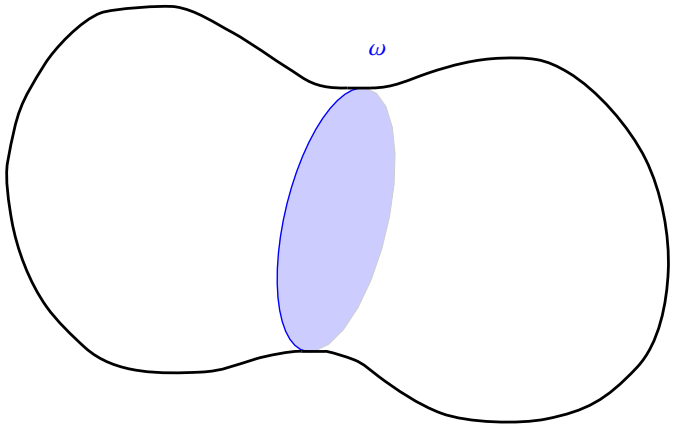

Figure 2: The structure without the layer of heterogeneities

2.2. The inner-outer matched asymptotic method

The presence of the heterogeneities involves a boundary layer effect, i.e. a significant variation of the solution near ω. The matched asymptotic expansion method applied to the present problem has the following steps:

- Decomposition of the domain Ω into two overlapping subdomains (see Fig. 3 and Fig. 4):
  - ⋆ the domain $\Omega^{out,\varepsilon} = \{\boldsymbol{x} = (x_1, x_2, x_3) \in \Omega;\ |x_1| > \frac{\varepsilon}{2}\}$,
  - ⋆ the domain $\Omega^{in,\varepsilon} = \{\boldsymbol{x} = (x_1, x_2, x_3) \in \Omega^{\varepsilon};\ |x_1| < \frac{\eta(\varepsilon)}{2}\}$ where $\eta(\varepsilon)$ is a function satisfying the following conditions:

$$\begin{cases} \lim\limits_{\varepsilon \to 0} \eta(\varepsilon) = 0 \\ \lim\limits_{\varepsilon \to 0} \dfrac{\eta(\varepsilon)}{\varepsilon} = +\infty \end{cases} \tag{3}$$

- Introduction of the normalized coordinate systems:

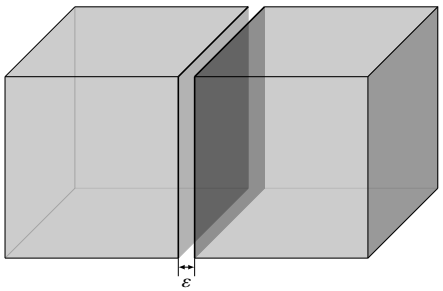

Figure 3: $\Omega^{out,\varepsilon} = \Omega^{+,\varepsilon} \cup \Omega^{-,\varepsilon}$

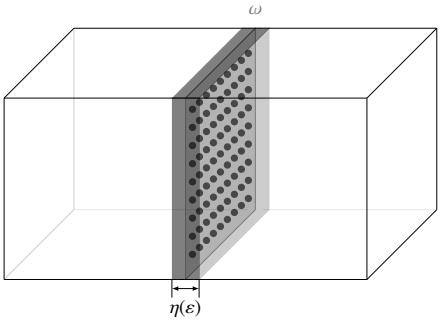

Figure 4: $\Omega^{in,\varepsilon}$

⋆ When $\varepsilon \to 0$, the domain $\Omega^{out,\varepsilon}$ tends to a fixed domain $\Omega^- \cup \Omega^+ = \Omega \setminus \omega = \{\boldsymbol{x} \in \Omega \ ; \ |x_1| > 0\}$ which is also called the *outer domain*. The outer system of coordinates is $\boldsymbol{x} := (x_1, x_2, x_3) \in \Omega \setminus \omega$.

⋆ Since ω is contained in the union of $\mathcal{N}(\varepsilon)$ sets $\varepsilon\hat{Y}$, as in the periodic homogenisation procedure the position $\boldsymbol{z} := (z_1, z_2, z_3)$ of a point M in the domain $\Omega^{in,\varepsilon}$ can be given by two independent data:
i) *the macroscopic position* $(0, \hat{\boldsymbol{x}}) := (0, x_2, x_3) \in \omega$ of the *center* of the period $\varepsilon\hat{Y}$ containing the projection of M on ω
ii) *the microscopic position* defined as the position of the point M with respect to this center. To obtain a domain and a coordinate system independent from ε, one applies a dilatation of the variables εy_i of a factor $\frac{1}{\varepsilon}$. Using (3) and the periodicity assumption on the heterogeneities, the *inner domain* is $\omega \times Y$ where $Y := \mathbb{R} \times \hat{Y}$ is called the basic cell (see Fig.5) and the relation between the

coordinates $\boldsymbol{z}$ of the point M and the point $((0, \hat{\boldsymbol{x}}), \boldsymbol{y})$ of the inner domain is given by:

$$\boldsymbol{z} = (0, \hat{\boldsymbol{x}}) + \varepsilon \boldsymbol{y}. \tag{4}$$

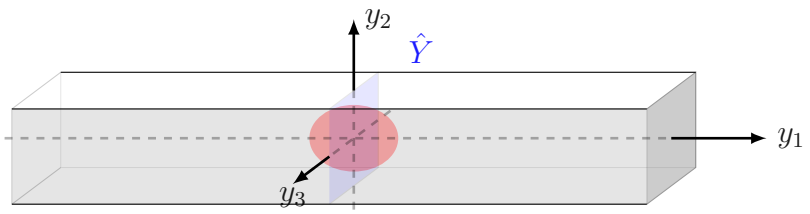

Figure 5: The basic cell Y

This correspondence implies that the operators divergence ($\boldsymbol{div}$) and symmetric gradient ($\boldsymbol{\gamma}$) must be reformulated in terms of the macroscopic $\hat{\boldsymbol{x}}$ and the microscopic $\boldsymbol{y} = (y_1, \hat{\boldsymbol{y}})$ coordinates in the following way:

$$\begin{aligned} \boldsymbol{div}\, \boldsymbol{\tau}(\hat{\boldsymbol{x}}, \boldsymbol{y}) &= \boldsymbol{div}_x \boldsymbol{\tau}(\hat{\boldsymbol{x}}, \boldsymbol{y}) + \frac{1}{\varepsilon} \boldsymbol{div}_y \boldsymbol{\tau}(\hat{\boldsymbol{x}}, \boldsymbol{y}) \\ \boldsymbol{\gamma}(\boldsymbol{v}(\hat{\boldsymbol{x}}, \boldsymbol{y})) &= \boldsymbol{\gamma}_{\boldsymbol{x}}(\boldsymbol{v}(\hat{\boldsymbol{x}}, \boldsymbol{y})) + \frac{1}{\varepsilon} \boldsymbol{\gamma}_{\boldsymbol{y}}(\boldsymbol{v}(\hat{\boldsymbol{x}}, \boldsymbol{y})) \end{aligned} \tag{5}$$

with:

$$\begin{cases} \boldsymbol{div}_x \boldsymbol{\tau} = \dfrac{\partial \tau_{ij}}{\partial x_j} \boldsymbol{e}_i & , \quad \boldsymbol{div}_y \boldsymbol{\tau} = \dfrac{\partial \tau_{ij}}{\partial y_j} \boldsymbol{e}_i \\ (\boldsymbol{\gamma}_x(\boldsymbol{v}))_{ij} = \dfrac{1}{2}\left(\dfrac{\partial v_j}{\partial x_i} + \dfrac{\partial v_i}{\partial x_j}\right) & , \quad (\boldsymbol{\gamma}_y(\boldsymbol{v}))_{ij} = \dfrac{1}{2}\left(\dfrac{\partial v_j}{\partial y_i} + \dfrac{\partial v_i}{\partial y_j}\right) \end{cases} \tag{6}$$

- Ansatz:
  Introduction of the two a priori asymptotic expansions of $\boldsymbol{u}^\varepsilon$:
  - ⋆ *the outer expansion*

$$\boldsymbol{u}^\varepsilon(x_1, x_2, x_3) = \sum_{i=0}^{\infty} \varepsilon^i \boldsymbol{u}^i(x_1, x_2, x_3) \tag{7}$$

⋆ *the inner expansion*

$$\boldsymbol{u}^{\varepsilon}(x_1, x_2, x_3) = \sum_{i=0}^{\infty} \varepsilon^i \boldsymbol{v}^i(\hat{\boldsymbol{x}}, y_1, \hat{\boldsymbol{y}}) \tag{8}$$

where the $\boldsymbol{v}^i$ are $\hat{Y}$-periodic, i.e. such that:

$$\boldsymbol{v}^i(\hat{\boldsymbol{x}}, y_1, \hat{\boldsymbol{y}} + p\boldsymbol{e}_2 + q\boldsymbol{e}_3) = \boldsymbol{v}^i(\hat{\boldsymbol{x}}, y_1, \hat{\boldsymbol{y}}) \quad \forall (p, q) \in \mathbb{Z}^2 \tag{9}$$

and $\hat{\boldsymbol{x}} \in \omega$ has to be considered as a parameter.

- Deduction of the outer and inner expansion of $\boldsymbol{\sigma}^{\varepsilon}$:
We use the constitutive equations and the inner and outer expansion of $\boldsymbol{u}^{\varepsilon}$ to determinate the outer and the inner expansion of $\boldsymbol{\sigma}^{\varepsilon}$. One has a priori to distinguish between the case of holes and the case of hyper-elastic inclusions characterized by the hyper-elastic fourth-order tensor $\boldsymbol{A}^{\varepsilon,I} = \varepsilon^p \boldsymbol{A}^I$ with $\boldsymbol{A}^I \backsimeq \boldsymbol{A}$ and $p \in \mathbb{N}$.

  ⋆ *Outer expansion.* Outside the heterogeneities the structure is constituted by a linearly hyper-elastic material whose rigidity tensor is $\boldsymbol{A}$, and hence:

$$\boldsymbol{\sigma}^{\varepsilon}(\boldsymbol{x}) = \sum_{i=0}^{\infty} \varepsilon^i \boldsymbol{\sigma}^i(\boldsymbol{x}) \tag{10}$$

with

$$\boldsymbol{\sigma}^i = \boldsymbol{A}\boldsymbol{\gamma}_x(\boldsymbol{u}^i) \tag{11}$$

  ⋆ *Inner expansion.* The distinction between the holes and the elastic inclusions is significant:

    ∗ in $Y \backslash I$ (for holes or elastic inclusions):

$$\boldsymbol{\sigma}^{\varepsilon}(\boldsymbol{x}) = \sum_{i=-1}^{\infty} \varepsilon^i \boldsymbol{\tau}^i(\hat{\boldsymbol{x}}, \boldsymbol{y}) \tag{12}$$

with

$$\begin{cases} \boldsymbol{\tau}^{-1} = \boldsymbol{A}\boldsymbol{\gamma}_y(\boldsymbol{v}^0) \\ \boldsymbol{\tau}^i \ = \boldsymbol{A}\boldsymbol{\gamma}_x(\boldsymbol{v}^i) + \boldsymbol{A}\boldsymbol{\gamma}_y(\boldsymbol{v}^{i+1}) \ \text{ for } \ i \geq 0 \end{cases} \tag{13}$$

$*$ in I (only for elastic inclusions):

$$\boldsymbol{\sigma}^{\varepsilon}(\boldsymbol{x}) = \sum_{i=p-1}^{\infty} \varepsilon^i \boldsymbol{\tau}^i(\hat{\boldsymbol{x}}, \boldsymbol{y}) \tag{14}$$

with

$$\begin{cases} \boldsymbol{\tau}^{p-1} = \boldsymbol{A}^I \boldsymbol{\gamma}_y(\boldsymbol{v}^0) \\ \boldsymbol{\tau}^i \quad = \boldsymbol{A}^I \boldsymbol{\gamma}_x(\boldsymbol{v}^{i-p}) + \boldsymbol{A}^I \boldsymbol{\gamma}_y(\boldsymbol{v}^{i-p+1}) \ \text{ for } \quad i \geq p \end{cases} \tag{15}$$

The fields $\boldsymbol{\tau}^i$ are $\hat{Y}$-periodic, with respect to $\hat{\boldsymbol{y}}$ and $\hat{\boldsymbol{x}} \in \omega$ has to be considered as a parameter.

- Deduce the boundary value problems verified by the different terms of the inner and outer expansion. In general the boundary value problems for the terms of the outer expansion need transmission conditions on ω that are not directly determined and the boundary value problems for the terms of the inner expansion may have a non unique solution.

- Provide matching conditions between the inner and the outer expansion in order to complete the statement of the transmission conditions on ω and to completely determine the inner solution.

Following these steps one can compute the terms of each asymptotic expansion; in our situation only the first two deserve attention. Let us explicitly remark that in the inner expansion the development of $\boldsymbol{\sigma}^{\varepsilon}$ begins with the term $\boldsymbol{\tau}^{-1}$ in $Y \backslash I$ and the term $\boldsymbol{\tau}^{p-1}$ in I.

2.2.1. Theoretical results for the asymptotic study

This section is a reminder without any proofs of the main results of the asymptotic study (see [1] for details).

Zeroth-order approximation: .

- inner approximation: the solution $\boldsymbol{v}^0$ verify

$$\boldsymbol{v}^0(\boldsymbol{x}, \boldsymbol{y}) = \boldsymbol{v}^0(\boldsymbol{x}) = \boldsymbol{u}^0(0, \hat{\boldsymbol{x}}) \tag{16}$$

where $\boldsymbol{u}^0$ is the solution of the outer approximation

- outer approximation: $\boldsymbol{u}^0$ is solution of

$$\begin{cases} \boldsymbol{div}\boldsymbol{\sigma}^0(\boldsymbol{u}^0) = \boldsymbol{0} & \text{in } \Omega_0 \\ \boldsymbol{\sigma}^0 = \boldsymbol{A}\boldsymbol{\gamma}(\boldsymbol{u}^0) & \text{in } \Omega_0 \\ \boldsymbol{\sigma}^0\boldsymbol{n} = \boldsymbol{F} & \text{on } \Gamma_F \\ \boldsymbol{u}^0 = \boldsymbol{0} & \text{on } \Gamma_0 \end{cases} \tag{17}$$

Remark 1: Notice that there are no jumps on ω for the outer approximation. In other words, at the zero order the outer approximation does not take into account the heterogeneities. Thus this problem can be solved using a standard finite element procedure.

Remark 2: Since $\boldsymbol{A}$ is constant (or regular), the classical regularity results for linear elasticity imply that the solution $\boldsymbol{u}^0$ is regular in $\overline{\Omega}\backslash(\overline{\Gamma_0} \cap \overline{\Gamma_F})$ and hence on $\overline{\omega}$ when $\partial\omega \cap (\overline{\Gamma_0} \cap \overline{\Gamma_F}) = \emptyset$.

First-order approximation: .

- inner approximation:
  - ⋆ The definition of $\boldsymbol{v}^1(\hat{\boldsymbol{x}}, \boldsymbol{y})$ is similar in the case of holes and in the case of elastic inclusions

$$\boldsymbol{v}^1(\hat{\boldsymbol{x}}, \boldsymbol{y}) = f(y_1; a, b)\frac{\partial \boldsymbol{u}^0}{\partial x_1}(0, \hat{\boldsymbol{x}}) + \frac{\partial u_i^0}{\partial x_j}(0, \hat{\boldsymbol{x}})\boldsymbol{V}^{ij}(\boldsymbol{y}) + \check{\boldsymbol{v}}(\hat{\boldsymbol{x}}) \tag{18}$$

    where: $f(y_1; a, b)$ is an odd function of class $\mathcal{C}^2(\mathbb{R})$ such that

$$f(y_1; a, b) = \begin{cases} 0 & \text{if } 0 < |y_1| \leq a \\ y_1 & \text{if } |y_1| \geq b \end{cases} \tag{19}$$

    with $d < 2a < 2b$ (in the sequel, except when we wish to stress the dependence on a, b, we will simply write $f(y_1)$). Let us only stress that in the case of holes $\boldsymbol{y} \in Y\backslash I$ and in the case of elastic inclusions $\boldsymbol{y} \in Y$.
  - ⋆ When $\boldsymbol{y} \in Y\backslash I$ the definition of $\boldsymbol{\tau}^0$ is the same for holes and for elastic inclusions and follows from (13) :

$$\boldsymbol{\tau}^0(\hat{\boldsymbol{x}}, \boldsymbol{y}) = \boldsymbol{G}(y_1, \boldsymbol{u}^0) + \frac{\partial u_i^0}{\partial x_j}(0, \hat{\boldsymbol{x}})\boldsymbol{A}\boldsymbol{\gamma}_y(\boldsymbol{V}^{ij})(\boldsymbol{y}) \tag{20}$$

where the tensor $\boldsymbol{G}$ is defined by

$$\boldsymbol{G}(y_1, \boldsymbol{u}^0) = \boldsymbol{A}\left(\boldsymbol{\gamma_x}\left(\boldsymbol{u}^0(0,\hat{\boldsymbol{x}})\right) + f'(y_1)\frac{\partial \boldsymbol{u}^0}{\partial x_1}(0,\hat{\boldsymbol{x}}) \otimes_S \boldsymbol{e}_1\right) \quad (21)$$

⋆ When $\boldsymbol{y} \in I$ then (14) and (15) imply that the definition of $\boldsymbol{\tau}^0$ depends on p. More precisely when $p \geq 1$ one has $\boldsymbol{\tau}^0 = 0$ and when $p = 0$ one has:

$$\boldsymbol{\tau}^0(\hat{\boldsymbol{x}}, \boldsymbol{y}) = \boldsymbol{G}(y_1, \boldsymbol{u}^0) + \frac{\partial u_i^0}{\partial x_j}(0,\hat{\boldsymbol{x}})\boldsymbol{A}\boldsymbol{\gamma}_y(\boldsymbol{V}^{ij})(\boldsymbol{y}) \quad (22)$$

where the tensor $\boldsymbol{G}$ is defined by

$$\boldsymbol{G}(y_1, \boldsymbol{u}^0) = \boldsymbol{A}^I\left(\boldsymbol{\gamma_x}\left(\boldsymbol{u}^0(0,\hat{\boldsymbol{x}})\right) + f'(y_1)\frac{\partial \boldsymbol{u}^0}{\partial x_1}(0,\hat{\boldsymbol{x}}) \otimes_S \boldsymbol{e}_1\right) \quad (23)$$

⋆ The fields $\boldsymbol{V}^{ij}$ are solution of the following cell problems for $p = 0$, resp. for $p \geq 1$ (or for the case of holes since the two situations give rise to the same equations):

i) for (l,1), l = 1, 2, 3:

$$\begin{cases} \boldsymbol{div}_y \boldsymbol{T}^{l1} = -f''(y_1)A_{i1l1}\boldsymbol{e}_i & \text{in } Y (\text{resp. in } Y\backslash I) \\ \boldsymbol{T}^{l1} = \boldsymbol{A}\boldsymbol{\gamma}_y(\boldsymbol{V}^{l1}) & \text{in } Y (\text{resp. in } Y\backslash I) \\ \boldsymbol{T}^{l1}(\hat{\boldsymbol{x}}, y_1, \frac{1}{2}, y_3)\boldsymbol{e}_2 = \boldsymbol{T}^{l1}(\hat{\boldsymbol{x}}, y_1, -\frac{1}{2}, y_3)\boldsymbol{e}_2 & \text{on } \mathbb{R}\times\partial\hat{Y} \\ \boldsymbol{T}^{l1}(\hat{\boldsymbol{x}}, y_1, y_2, \frac{1}{2})\boldsymbol{e}_3 = \boldsymbol{T}^{l1}(\hat{\boldsymbol{x}}, y_1, y_2, -\frac{1}{2})\boldsymbol{e}_3 & \text{on } \mathbb{R}\times\partial\hat{Y} \\ \boldsymbol{V}^{l1}(\hat{\boldsymbol{x}}, y_1, \frac{1}{2}, y_3) = \boldsymbol{V}^{l1}(\hat{\boldsymbol{x}}, y_1, -\frac{1}{2}, y_3) & \text{on } \mathbb{R}\times\partial\hat{Y} \\ \boldsymbol{V}^{l1}(\hat{\boldsymbol{x}}, y_1, y_2, \frac{1}{2}) = \boldsymbol{V}^{l1}(\hat{\boldsymbol{x}}, y_1, y_2, -\frac{1}{2}) & \text{on } \mathbb{R}\times\partial\hat{Y} \\ \lim\limits_{y_1\to\pm\infty} \boldsymbol{T}^{l1}(y_1, \hat{\boldsymbol{y}})\boldsymbol{e}_1 = \boldsymbol{0} & \text{for } \hat{\boldsymbol{y}} \in \hat{Y} \end{cases} \quad (24)$$

with the transmission or boundary conditions on ∂I:

elastic inclusions ($p = 0$)	elastic inclusion ($p > 0$) holes
$[\boldsymbol{V}^{l1}] = [\boldsymbol{T}^{l1}\boldsymbol{n}] = \boldsymbol{0}$	$\boldsymbol{T}^{l1}\boldsymbol{n} = \boldsymbol{0}$

(25)

ii) for (l,k) = (1,2) ; (2,2) ; (3,2) ; (1,3) ; (2,3) ; (3,3),

$$\begin{cases} \boldsymbol{div}_y \boldsymbol{T}^{lk} = \boldsymbol{0} & \text{in } Y (\text{resp. in } Y \backslash I) \\ \boldsymbol{T}^{lk} = \boldsymbol{A}\boldsymbol{\gamma}_y(\boldsymbol{V}^{lk}) & \text{in } Y (\text{resp. in } Y \backslash I) \\ \boldsymbol{T}^{lk}(\hat{\boldsymbol{x}}, y_1, \frac{1}{2}, y_3)\boldsymbol{e}_2 = \boldsymbol{T}^{lk}(\hat{\boldsymbol{x}}, y_1, -\frac{1}{2}, y_3)\boldsymbol{e}_2 & \text{on } \mathbb{R} \times \partial\hat{Y} \\ \boldsymbol{T}^{lk}(\hat{\boldsymbol{x}}, y_1, y_2, \frac{1}{2})\boldsymbol{e}_3 = \boldsymbol{T}^{lk}(\hat{\boldsymbol{x}}, y_1, y_2, -\frac{1}{2})\boldsymbol{e}_3 & \text{on } \mathbb{R} \times \partial\hat{Y} \\ \boldsymbol{V}^{lk}(\hat{\boldsymbol{x}}, y_1, \frac{1}{2}, y_3) = \boldsymbol{V}^{lk}(\hat{\boldsymbol{x}}, y_1, -\frac{1}{2}, y_3) & \text{on } \mathbb{R} \times \partial\hat{Y} \\ \boldsymbol{V}^{lk}(\hat{\boldsymbol{x}}, y_1, y_2, \frac{1}{2}) = \boldsymbol{V}^{lk}(\hat{\boldsymbol{x}}, y_1, y_2, -\frac{1}{2}) & \text{on } \mathbb{R} \times \partial\hat{Y} \\ \lim\limits_{y_1 \to \pm\infty} \boldsymbol{T}^{lk}(y_1, \hat{\boldsymbol{y}})\boldsymbol{e}_1 = \boldsymbol{0} & \text{for } \hat{\boldsymbol{y}} \in \hat{Y} \end{cases} \tag{26}$$

with the transmission or boundary conditions on ∂I:

elastic inclusions ($p = 0$)	elastic inclusion ($p > 0$) holes
$[\boldsymbol{V}^{lk}] = \boldsymbol{0}$ $[\boldsymbol{T}^{lk}\boldsymbol{n}] = ((\boldsymbol{A}^I - \boldsymbol{A})(\boldsymbol{e}_l \otimes_S \boldsymbol{e}_k))\boldsymbol{n}$	$\boldsymbol{T}^{lk}\boldsymbol{n} = -\left(A_{ijlk} n_j\right) \boldsymbol{e}_i$

(27)

Remark 3: For the problems (24) and (26), the following asymptotic behavior holds:

$$\lim_{y_1 \to \pm\infty} \boldsymbol{V}^{ij}(y_1, \hat{\boldsymbol{y}}) = \boldsymbol{V}^{ij\pm} \tag{28}$$

Furthermore, the solutions of the cell problems are only defined up to a translation. The uniqueness of $\boldsymbol{V}^{ij}$ can be recovered by adding the following condition:

$$\boldsymbol{V}^{ij+} + \boldsymbol{V}^{ij-} = \boldsymbol{0} \tag{29}$$

Remark 4: The inner term $\boldsymbol{\tau}^0$ is completely determined by the computation of the cell problems while (18) implies that $\boldsymbol{v}^1$ requires the calculation of the constant $\check{\boldsymbol{v}}$. This constant will be determined once $\boldsymbol{u}^1$ is known by the following relation:

$$\check{\boldsymbol{v}}(\hat{\boldsymbol{x}}) = \frac{1}{2}(\boldsymbol{u}^1(0^+, \hat{\boldsymbol{x}}) + \boldsymbol{u}^1(0^-, \hat{\boldsymbol{x}})) \tag{30}$$

Let us also remark that in the case $p = 1$ (24), (26) and (30) allow to compute $\boldsymbol{v}^1(\hat{\boldsymbol{x}}, y_1, \hat{\boldsymbol{y}})$ only in $Y \backslash I$. In order to find the displacement

field $\boldsymbol{v}^1$ in all Y we remark that in I it is the unique solution of the elasticity problem with Dirichlet boundary conditions:

$$\begin{cases} \boldsymbol{div}_y \boldsymbol{A}^I \boldsymbol{\gamma}_y(\boldsymbol{v}^1) = 0 & \text{in } \ I \\ \boldsymbol{v}^1 = \dfrac{\partial u_l^0}{\partial x_k}(0, \hat{\boldsymbol{x}}) \boldsymbol{V}^{lk}(\boldsymbol{y}) + \check{\boldsymbol{v}}(\hat{\boldsymbol{x}}) & \text{on } \ \partial I \end{cases} \tag{31}$$

- outer approximation:
  The outer term $\boldsymbol{u}^1$ is the solution of the following boundary value problem:

$$\begin{cases} \boldsymbol{div}\boldsymbol{\sigma}^1 = \boldsymbol{0} & \text{in } \Omega_0 \backslash \omega \\ \boldsymbol{\sigma}^1 = \boldsymbol{A}\boldsymbol{\gamma}(\boldsymbol{u}^1) & \text{in } \Omega_0 \backslash \omega \\ \boldsymbol{\sigma}^1 \boldsymbol{n} = \boldsymbol{0} & \text{on } \Gamma_F \\ \boldsymbol{u}^1 = \boldsymbol{0} & \text{on } \Gamma_0 \end{cases} \tag{32}$$

  and the transmissions conditions on ω :

$$\begin{cases} \left[\boldsymbol{u}^1\right](\hat{\boldsymbol{x}}) = \boldsymbol{\mathcal{G}_d}\left(\boldsymbol{u}^0(0, \hat{\boldsymbol{x}}) \ ; \left[\boldsymbol{V}^{ij}\right]^\infty\right) \\ \left[\boldsymbol{\sigma}^1 \boldsymbol{e}_1\right](\hat{\boldsymbol{x}}) = \boldsymbol{\mathcal{G}_{nS}}\left(\boldsymbol{u}^0(0, \hat{\boldsymbol{x}}) \ ; \displaystyle\int_Y \boldsymbol{T}^{ij}(\boldsymbol{y}) \ d\boldsymbol{y}\right) \end{cases}$$

  where

$$\left[\boldsymbol{V}^{ij}\right]^\infty = \boldsymbol{V}^{ij+} - \boldsymbol{V}^{ij-}$$

  For the different types of inclusions considered, one has:

$$\boldsymbol{\mathcal{G}_d} = \frac{\partial u_i^0}{\partial x_j}(0, \hat{\boldsymbol{x}}) \left[\boldsymbol{V}^{ij}\right]^\infty \tag{33}$$

  The expression of $\boldsymbol{\mathcal{G}_{nS}}$ depends on the inclusion:

  i) in the elastic inclusions case one has:

$$\boldsymbol{\mathcal{G}_{nS}} = \boldsymbol{div}_x \left(|I| \left(\boldsymbol{A} - \boldsymbol{A}^I\right) \boldsymbol{\gamma}_x \left(\boldsymbol{u}^0(0, \hat{\boldsymbol{x}})\right) - \frac{\partial u_i^0}{\partial x_j}(0, \hat{\boldsymbol{x}}) \int_Y \boldsymbol{T}^{ij}(\boldsymbol{y}) \ d\boldsymbol{y} \right) \tag{34}$$

  ii) in the holes case one has:

$$\boldsymbol{\mathcal{G}_{nS}} = \boldsymbol{div}_x \left(|I| \boldsymbol{A} \boldsymbol{\gamma}_x \left(\boldsymbol{u}^0(0, \hat{\boldsymbol{x}})\right) - \frac{\partial u_i^0}{\partial x_j}(0, \hat{\boldsymbol{x}}) \int_Y \boldsymbol{T}^{ij}(\boldsymbol{y}) \ d\boldsymbol{y} \right) \tag{35}$$

Remark 5: In practice, an efficient way to implement the jumping conditions in problem (32) is to solve this problem by a domain decomposition type algorithm. The actual procedure will be detailed in section 3.

2.3. Definition of the outer and inner approximations

Once determined the different terms $\mathbf{u}^i$ and $\mathbf{v}^i$ one can define an outer and an inner approximation of order m:

$$\mathbf{u}_m^{out} := \sum_{i=0}^{i=m} \varepsilon^i \mathbf{u}^i \tag{36}$$

$$\mathbf{u}_m^{inn} := \sum_{i=0}^{i=m} \varepsilon^i \mathbf{v}^i \tag{37}$$

The quality of these approximations increases with m; in our situation we only consider the cases $m = 0$ and $m = 1$.

3. Solution of the first order problem by domain decomposition

The first order problem (32) will be solved by a domain decomposition type algorithm. In order to describe this method we first recall (see e.g. [16]) the starting point for solving a standard linear elasticity problem by domain decomposition and then we adapt the solution procedure to this particular problem.

3.1. A linear elasticity model problem

As it is well known, under the usual symmetry and coercivity assumptions on $\boldsymbol{A}$, the following linear elasticity problem has a unique solution $\boldsymbol{u} \in \boldsymbol{H}^1(\Omega)$:

$$\left\{ \begin{array}{lcll} -\boldsymbol{div}\boldsymbol{\sigma} & = & \mathbf{f}^{\Omega} & \text{in } \Omega \\ \boldsymbol{\sigma} & = & \boldsymbol{A}\boldsymbol{\gamma}(\boldsymbol{u}) & \text{in } \Omega \\ \boldsymbol{\sigma}\boldsymbol{n} & = & \mathbf{F} & \text{on } \Gamma_F \\ \boldsymbol{u} & = & \mathbf{u}^d & \text{on } \Gamma_0 \end{array} \right. \tag{38}$$

Let the domain Ω be decomposed in two non overlapping subdomains Ω_1 and Ω_2 and let ω be the interface between the subdomains. The objective of the domain decomposition method is to replace the problem on the whole domain by a problem formulated on the interface. The two following conditions hold on the interface:

- continuity of the solution $\boldsymbol{u}$
- continuity of the normal stress

We'll impose one condition and verify the second. In the following to underline the (linear) dependence on $\boldsymbol{u}$ we set $\boldsymbol{\sigma}(\boldsymbol{u}) := \boldsymbol{A\gamma}(\boldsymbol{u})$. Let's define $\boldsymbol{\lambda} = Tr(\boldsymbol{u})$ on the interface ω where $\boldsymbol{u}$ denotes the solution of problem (38). Solve the problem (38) is equivalent to solve, on each subdomain, the following problems

$$\left\{\begin{array}{lcll} \boldsymbol{div\sigma}(\boldsymbol{u}^i) & = & \mathbf{f}^\Omega & \text{in } \Omega_i \\ \boldsymbol{\sigma}(\boldsymbol{u}^i) & = & \boldsymbol{A\gamma}(\boldsymbol{u}^i) & \text{in } \Omega_i \\ \boldsymbol{\sigma}(\boldsymbol{u}^i)\boldsymbol{n} & = & \mathbf{F} & \text{on } \Gamma_F \cap \Omega_i \\ \mathbf{u}^i & = & \mathbf{u}^d & \text{on } \Gamma_0 \cap \Omega_i \\ \mathbf{u}^i & = & \boldsymbol{\lambda} & \text{on } \omega \end{array}\right. \tag{39}$$

where $\boldsymbol{\lambda}$ is an additional unknown that must be determined in such a way that the normal stresses be continuous on the interface ω, i. e. since $\boldsymbol{n}^1 = -\boldsymbol{n}^2$:

$$\boldsymbol{\sigma}(\boldsymbol{u}^1)\boldsymbol{n}^1 + \boldsymbol{\sigma}(\boldsymbol{u}^2)\boldsymbol{n}^2 = 0 \tag{40}$$

On each subdomain Ω_i we define the Steklov-Poincaré operator S_i as follows: for $\boldsymbol{\lambda}$ given $\mathbf{u}_\lambda^i$ is the solution of

$$\left\{\begin{array}{lcll} \boldsymbol{div\sigma}(\mathbf{u}_\lambda^i) & = & 0 & \text{in } \Omega_i \\ \boldsymbol{\sigma}(\mathbf{u}_\lambda^i) & = & \boldsymbol{A\gamma}(\mathbf{u}_\lambda^i) & \text{in } \Omega \\ \boldsymbol{\sigma}(\mathbf{u}_\lambda^i)\boldsymbol{n}^i & = & 0 & \text{on } \Gamma_F \cap \Omega_i \\ \mathbf{u}_\lambda^i & = & \mathbf{u}^d & \text{on } \Gamma_0 \cap \Omega_i \\ \mathbf{u}_\lambda^i & = & \boldsymbol{\lambda} & \text{on } \omega \end{array}\right. \tag{41}$$

and S_i is defined by:

$$S_i\boldsymbol{\lambda} = \boldsymbol{\sigma}(\mathbf{u}_\lambda^i)\boldsymbol{n}^i$$

where $\boldsymbol{n}^i$ denotes the outer normal to Ω_i on ω.

Notice that using the linearity of (39) one has $\boldsymbol{u}^i = \boldsymbol{u}_0^i + \boldsymbol{u}_\lambda^i$ where $\boldsymbol{u}_0^i$ is solution of (39) with $\boldsymbol{u}_0^i = 0$ on ω. The continuity of the normal stress (40) gives

$$\boldsymbol{\sigma}(\mathbf{u}_\lambda^1)\boldsymbol{n}^1 + \boldsymbol{\sigma}(\boldsymbol{u}_0^1)\boldsymbol{n}^1 + \boldsymbol{\sigma}(\mathbf{u}_\lambda^2)\boldsymbol{n}^2 + \boldsymbol{\sigma}(\boldsymbol{u}_0^2)\boldsymbol{n}^2 = 0.$$

After introducing the Steklov-Poincaré operators we have

$$S_1\boldsymbol{\lambda} + S_2\boldsymbol{\lambda} = -\boldsymbol{\sigma}(\mathbf{u}_0^1)\boldsymbol{n}^1 - \boldsymbol{\sigma}(\mathbf{u}_0^2)\boldsymbol{n}^2$$

and finally, setting $S = S_1 + S_2$ the system on the interface becomes

$$S\boldsymbol{\lambda} = -\boldsymbol{\sigma}(\mathbf{u}_0^1)\boldsymbol{n}^1 - \boldsymbol{\sigma}(\mathbf{u}_0^2)\boldsymbol{n}^2 \tag{42}$$

Remark 1: The operators S_i are linear and continuous from $\boldsymbol{V}(\omega)$ into its dual $\boldsymbol{V}'(\omega)$. The definition of these spaces depends on the geometry of ω. When ω is a closed Lipschitz surface with no intersection with $\partial\Omega$ then $\boldsymbol{V}(\omega) = \boldsymbol{H}^{1/2}(\omega)$. Since $\boldsymbol{H}^{1/2}(\omega) \subset \boldsymbol{L}^2(\omega) := \boldsymbol{H}$ with continuous and dense imbedding one can take $\boldsymbol{H} \simeq \boldsymbol{H}'$ as pivot space and then $\boldsymbol{V}'(\omega) = \boldsymbol{H}^{-1/2}(\omega)$. When $\omega \cap \partial\Omega \neq \varnothing$ then an analogous construction is also possible but presents some technical difficulties.

Remark 2: S is a symmetric positive defined operator which, after discretization, gives the Schur complement. This operator is not known directly and is rather difficult to construct but the product $S\boldsymbol{\lambda}$ is easy to compute as it requires the solution of one problem by subdomain. It is thus convenient to solve the linear system by an iterative method as conjugate gradient or GMRES. GMRES is preferred for its robustness. In addition we'll note that even when CG is used a re-orthogonalisation is mandatory for such problems [17].

Remark 3: What was described in this section is only the starting point for a primal domain decomposition method. Several choices of preconditioners are available and the efficiency of the algorithm is indeed strongly depending on this choice. There is a vast literature on the subject, see e.g. [16]. We will use the Neumann-Neumann algorithm which was intensively studied and proved to be robust, [16], [18]. An alternative is to use a dual method of FETI type [19].

3.2. Solution of the first order problem

The script 1 which indicates the first order problem is omitted hereafter. The generic form of the first order problem (32) is given by:

$$\left\{\begin{array}{lcll} -\boldsymbol{div}\boldsymbol{\sigma}(\boldsymbol{u}) & = & \mathbf{0} & \text{in } \Omega \\ \boldsymbol{\sigma}(\boldsymbol{u}) & = & \boldsymbol{A}\boldsymbol{\gamma}(\boldsymbol{u}) & \text{in } \Omega \\ \boldsymbol{\sigma}(\boldsymbol{u})\boldsymbol{n} & = & \mathbf{0} & \text{on } \partial\Omega_F \\ \boldsymbol{u} & = & \mathbf{0} & \text{on } \partial\Omega_u \\ [\boldsymbol{u}] & = & \boldsymbol{\mathcal{G}_d} & \text{on } \omega \\ [\boldsymbol{\sigma}(\boldsymbol{u})\boldsymbol{n}] & = & \boldsymbol{\mathcal{G}_{nS}} & \text{on } \omega \end{array}\right. \tag{43}$$

where $\boldsymbol{\mathcal{G}_d}$ and $\boldsymbol{\mathcal{G}_{nS}}$ denote the gap in displacements, respectively normal stresses on ω. These data are known and can be computed once the zero order problem is solved. It should noted that the solution $\boldsymbol{u}$ of (43) does not belong to $\boldsymbol{H}^1(\Omega)$. More precisely, let be $\Omega_1 := \Omega^+$, $\Omega_2 := \Omega^-$ and :

$$\boldsymbol{Z}_0 := \{\boldsymbol{z} \in \boldsymbol{L}^2(\Omega); \boldsymbol{div}\boldsymbol{A}\boldsymbol{\gamma}(\boldsymbol{z}|_{\Omega_i}) = 0; \}; \tag{44}$$

then $\boldsymbol{u} \in \boldsymbol{Z}_0$. Hence the transmission conditions $[\boldsymbol{u}] = \boldsymbol{\mathcal{G}_d}$ and $[\boldsymbol{\sigma}(\boldsymbol{u})\boldsymbol{n}] = \boldsymbol{\mathcal{G}_{nS}}$ on ω have to be taken in a weak sense adapting the methods of Lions-Magenes [20] In the Appendix we briefly recall how this can be done.

The actual computation of $\boldsymbol{\mathcal{G}_d}$ and $\boldsymbol{\mathcal{G}_{nS}}$ will be described later on, see 3.3; the objective here is to transform the problem in order to obtain a domain decomposition as in (39).

The scripts in the following formulae indicates the subdomain number. Let $\boldsymbol{z}^i$ be the solution of the following problem:

$$\left\{\begin{array}{lcll} -\boldsymbol{div}\boldsymbol{\sigma}(\boldsymbol{z}^i) & = & \boldsymbol{0} & \text{in } \Omega_i \\ \boldsymbol{\sigma}(\boldsymbol{z}^i) & = & \boldsymbol{A}\boldsymbol{\gamma}(\boldsymbol{z}^i) & \text{in } \Omega_i \\ \boldsymbol{\sigma}(\boldsymbol{z}^i)\boldsymbol{n} & = & \boldsymbol{0} & \text{on } \partial\Omega_F \cap \Omega_i \\ \boldsymbol{z}^i & = & \boldsymbol{0} & \text{on } \partial\Omega_u \cap \Omega_i \\ \boldsymbol{z}^i & = & \boldsymbol{\mathcal{G}_d} & \text{on } \omega \end{array}\right. \tag{45}$$

Note that these are two independent problems. Thereafter, on each subdomain, we will look for a solution $\boldsymbol{u}^i$ which takes the following form:

$$\boldsymbol{u}^i = \boldsymbol{w}^i + \beta_i \boldsymbol{z}^i$$

with β_i two real numbers conveniently chosen. This can be done because the operator considered is linear. With these notations the new unknown of the problem is $\boldsymbol{w}^i$. Notice that $-\boldsymbol{div}\boldsymbol{\sigma}(\boldsymbol{w}^i) = 0$ and that the transmission conditions on ω for $\boldsymbol{w}^i$ are given by:

$$\left\{\begin{array}{l} [\boldsymbol{w}] = [\boldsymbol{u}] - \beta_1\boldsymbol{\mathcal{G}_d} + \beta_2\boldsymbol{\mathcal{G}_d} = (1 - \beta_1 + \beta_2)\boldsymbol{\mathcal{G}_d} \\ [\boldsymbol{\sigma}(\boldsymbol{w})\boldsymbol{n}] = [\boldsymbol{\sigma}(\boldsymbol{u})\boldsymbol{n}] + \beta_1\boldsymbol{\sigma}(\boldsymbol{z}^1)\boldsymbol{n} - \beta_2\boldsymbol{\sigma}(\boldsymbol{z}^2)\boldsymbol{n} = \boldsymbol{\mathcal{G}_{nS}} + \beta_1\boldsymbol{\sigma}(\boldsymbol{z}^1)\boldsymbol{n} - \beta_2\boldsymbol{\sigma}(\boldsymbol{z}^2)\boldsymbol{n} \end{array}\right.$$

If we choose $1 - \beta_1 + \beta_2 = 0$ then $\boldsymbol{w}$ is continuous on the interface ω but the normal stress is not and it is the unique non-homogeneous data. As in section 3.1 using the Steklov-Poincaré operator the problem to solve on the interface is

$$S\boldsymbol{\lambda} = \boldsymbol{\mathcal{G}_{nS}} + \beta_1\boldsymbol{\sigma}(\boldsymbol{z}^1)\boldsymbol{n}^1 - \beta_2\boldsymbol{\sigma}(\boldsymbol{z}^2)\boldsymbol{n}^2$$

which can also be written as:

$$S\lambda = -\boldsymbol{\sigma}(\boldsymbol{w}_0^1)\boldsymbol{n}^1 - \boldsymbol{\sigma}(\boldsymbol{w}_0^2)\boldsymbol{n}^2 + \boldsymbol{\mathcal{G}_{nS}} + \beta_1\ S_1\boldsymbol{\mathcal{G}_d} - \beta_2\ S_2\boldsymbol{\mathcal{G}_d} \tag{46}$$

Notice that equations (42) and (46) differ only on the right hand side. Thus as the operator does not change, the same algorithms may be used to solve the problem with the same performance and no additional analysis is required to prove efficiency.

3.3. Implementation issues

In the framework of domain decomposition algorithms, the implementation of the problem (43) is straightforward as it only requires the solution of an additional problem by subdomain. This problem is of the same type as the standard ones solved by the algorithm.

If we come back to the original equation into consideration (32) the only remaining problem is to compute the input data for the domain decomposition algorithm, that is the right hand sides for the jumps.

$$\left\{\begin{array}{rcl} \boldsymbol{\mathcal{G}_d} & = & \boldsymbol{\mathcal{G}_d}\left(\dfrac{\partial u_i}{\partial x_j}(0,\hat{\boldsymbol{x}})\ ;\ \left[\boldsymbol{V}^{ij}\right]^{\infty}\right) \\ \\ \boldsymbol{\mathcal{G}_{nS}} & = & \boldsymbol{\mathcal{G}_{nS}}\left(\dfrac{\partial^2 u_i}{\partial x_\alpha \partial x_j}(0,\hat{\boldsymbol{x}})\ ;\ \displaystyle\int_Y \boldsymbol{T}^{ij}(\boldsymbol{y})\ d\boldsymbol{y}\right) \end{array}\right. \tag{47}$$

From a mathematical point of view these quantities are data as they depend on the solution of the zero order problem. From a computational point of view this task is rather delicate. Indeed the solution of the zero order problem was obtained by a standard finite element method. So the solution $\boldsymbol{u}^0$ is $\mathcal{C}^0$ that means no continuity of the derivatives. The actual computations require first order derivatives for stresses that means second order derivatives for displacements. As it is well known, see e.g [21] Chap. 4, Sec 4.2, the calculation of derivatives numerically is a hazardous operation since it is inherently sensitive, as small perturbations in data can cause large changes in result (in other words numerical differentiation is ill-conditioned). For this reason, to approximate derivative of a function whose values are known only at discrete set of points, a good approach is to fit some smooth function to given data and then differentiate the approximating function. If the given data are sufficiently smooth, then interpolation may be appropriate; here $\boldsymbol{u}^0 \in \mathcal{C}^0$ and hence it is worth regularizing before computing

derivatives. Let us remark, with [21], Chap 6, Sect 6.7 that the choice of the better approximation "is in the realm of the art rather than in the science of numerical analysis. Intuition - meaning experience, really - and general physical knowledge of the problem must be used."

- **computation of $\boldsymbol{\mathcal{G}_d}$**

  In practice the value of the displacement derivative at a node is a weighted average of the values of the different elements containing the node.

- **computation of $\boldsymbol{\mathcal{G}_{nS}}$**

  Let's first notice that, for the sake of simplicity, all equations appear as partial differential equations, instead of in variational form. What is needed in practice, once the variational form is introduced, is $\int_\Gamma \boldsymbol{\mathcal{G}_{nS}} v dv$. As the integral is computed element by element at a first glance it is not mandatory to regularize before integrating. Nevertheless our choice was to use the same regularization as for the computation of $\boldsymbol{\mathcal{G}_d}$.

4. Validation

The objective of the validation is to study, in an appropriate norm, the error between the exact solution and the solution obtained by asymptotic expansions (zero order and first order). This error depends both on $\boldsymbol{u}_h^\varepsilon$ and h the discretisation step. Our interest is to focus on the dependence of the error of ε and h. So for all the computations the approximation error (which depends on h) has to be negligible, in other words h has to be much smaller then ε. Hence there are several difficulties in the validation process:

i) *The domain depends on the value of ε.* For the test problem and for decreasing values of ε the number of heterogeneities increases, thus the domain changes and it is impossible to obtain an uniform refinement of the mesh with respect to ε.

ii) *The analytical solution of the original test problem is not known.* We use instead a reference solution $\boldsymbol{u}_h^\varepsilon$ obtained with standard $P2$ finite elements on a suitable mesh Ω_h^ε, fine enough so that the error between the exact solution and the computed one is negligible in comparison

with the error due to the use of asymptotic expansions. Let us recall that when the solution $\boldsymbol{u}^\varepsilon$ has enough regularity the H^1 norm is used to measure the error and one has, for a fixed ε and for a regular mesh with discretization step h: $\|\boldsymbol{u}^\varepsilon - \boldsymbol{u}_h^\varepsilon\|_{H^1(\Omega^\varepsilon)} \leq Ch^2$. The solution of our target problem is not regular enough, this is why an L^2 norm will be preferred as detailed here in Sect. 4.3

iii) *The definition of* $\Omega^{in,\varepsilon}$ *depends on* $\eta(\varepsilon)$. The function $\eta(\varepsilon)$ is not given, it must only verify (3) and it has a crucial importance on the overlap.

iv) *The boundary of the domain* Ω *has corners*: the numerical solution of the different problems has boundary layers whose effects can perturb the quality of the results.

Taking into account these difficulties the validation is achieved trough the following steps:

1. Description of the test problem
2. Numerical solution of the cell problem
3. Validation at the macroscopic scale
4. Validation at the microscopic scale

4.1. Description of the test problem

Let $\Omega = (-L, L) \times (-H, H)$ be a plane domain containing $\mathcal{N}(\varepsilon) = 2H\varepsilon^{-1}$ identical discs of radius εR, arranged periodically (with period ε), along the line ω of equation $x_1 = 0$; let us remark that hence $d = 2R$. Outside the heterogeneities the structure is constituted of an elastic homogeneous isotropic material, characterized by its Young modulus E and Poisson coefficient ν. The boundary Γ_0 of the structure is clamped and a density $\boldsymbol{F}$ of linear force is applied on the complementary part Γ_F. There are no body forces (see Fig. 6). We will consider a 2D plane stress problem. The heterogeneities can be holes or elastic inclusions; in this case the elastic homogeneous isotropic material forming the heterogeneities is characterized by the Young modulus $E^{\varepsilon,I} = \varepsilon^p E^I$ and the Poisson coefficient $\nu^{\varepsilon,I} = \nu$. In all cases the problem is solved by a standard $P2$ finite element method and we take $L = 1$ and $H = 0.5$.

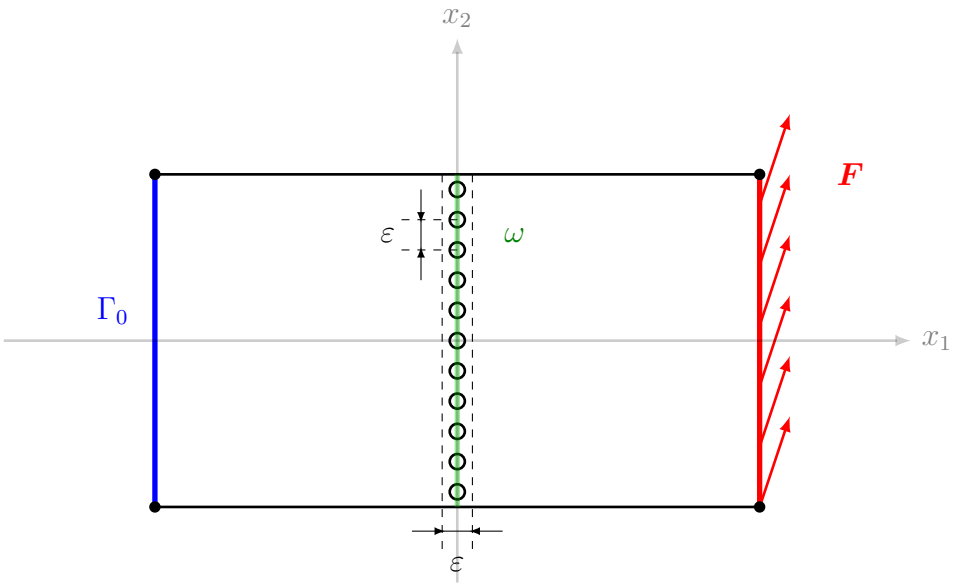

Figure 6: Test Problem

4.2. Numerical solution of the cell problems

The transmission conditions of the first-order outer problem (32) depend on the function $f(y_1)$ and on the solution of the cell problems posed on the unbounded domain Y. In practice we will use a bounded domain $Y_{L^\infty} =]\frac{-L^\infty}{2}, \frac{L^\infty}{2}[\times]\frac{-1}{2}, \frac{1}{2}[$ with a $L^\infty > 0$ big enough. The domain Y_{L^∞} contains a circular heterogeneity of radius R and centred at the origin. At first we numerically study, in the case of elastic inclusions with $p = 0$ and in the case of holes (or of elastic inclusions with $p > 1$), the robustness of the coefficients $[\boldsymbol{V}^{ij}]$ and $\int_Y \boldsymbol{T}^{ij} d\boldsymbol{y}$ with respect to:

i) the size L^∞ needed to approximate Y for the computation of $\boldsymbol{V}^{ij}$,

ii) the choice of the function $f(y_1)$,

iii) the choice of the radius R,

iv) In the case of elastic inclusions with $p = 0$ the dependence on E^I/E.

The cell problems (24)-(27) are solved by a standard P2 finite elements method.

4.2.1. Dependence on L^∞

The cell problems are solved by gradually increasing the length value L^∞. As odd function of class $\mathcal{C}^2(\mathbb{R})$ satisfying (19) a polynomial of order 5 for $a \leq |y_1| \leq b$ is choosed. The results are obtained with $R = 0.30$, $a = 1.5$, $b = 3a$, $E = 1$, $\nu = 0.25$ (and also with $E^I = 0.5$, $\nu^I = 0.25$ in the case $p = 0$). They show that for $L^\infty \geq 2.01b$ the coefficients $[\boldsymbol{V}^{ij}]$ and $\int_Y \boldsymbol{T}^{ij} d\boldsymbol{y}$ are stable (see Tables 1, 2, 3 and 4 below where only non-zero coefficients are given).

L^∞	$[V_1^{11}]^\infty$	$[V_2^{12}]^\infty$	$[V_2^{21}]^\infty$	$[V_1^{22}]^\infty$
2b+ 0.001b	0.2211195	0.2420530	0.2420514	0.0562849
2b+ 0.005b	0.2211221	0.2420530	0.2420524	0.0562849
2b+ 0.010b	0.2211242	0.2420530	0.2420527	0.0562849
2b+ 0.020b	0.2211258	0.2420530	0.2420527	0.0562849
2b+ 0.030b	0.2211261	0.2420530	0.2420527	0.0562849
2b+ 0.040b	0.2211262	0.2420530	0.2420527	0.0562849
2b+ 0.050b	0.2211262	0.2420530	0.2420527	0.0562849
2b+ 0.060b	0.2211262	0.2420530	0.2420527	0.0562849
2b+ 0.070b	0.2211262	0.2420530	0.2420527	0.0562849
2b+ 0.080b	0.2211262	0.2420530	0.2420527	0.0562849
2b+ 0.090b	0.2211262	0.2420530	0.2420527	0.0562849
2b+ 0.100b	0.2211262	0.2420530	0.2420527	0.0562849

Table 1: Variation of $[V_k^{ij}]^\infty$ with L^∞: elastic inclusions case

L^∞	$\int_Y T_{22}^{11} d\boldsymbol{y}$	$\int_Y T_{12}^{12} d\boldsymbol{y}$	$\int_Y T_{11}^{22} d\boldsymbol{y}$	$\int_Y T_{22}^{22} d\boldsymbol{y}$
2b+ 0.001b	-0.0010703	0.0561855	0.0374570	-0.0296238
2b+ 0.005b	-0.0010703	0.0561855	0.0374570	-0.0296238
2b+ 0.010b	-0.0010703	0.0561855	0.0374570	-0.0296238
2b+ 0.050b	-0.0010703	0.0561855	0.0374570	-0.0296238
2b+ 0.100b	-0.0010703	0.0561855	0.0374570	-0.0296238

Table 2: Variation of $\int_Y T_{kl}^{ij} d\boldsymbol{y}$ with L^∞: elastic inclusions case

L^∞	$[V_1^{11}]^\infty$	$[V_2^{12}]^\infty$	$[V_2^{21}]^\infty$	$[V_1^{22}]^\infty$
2b+ 0.001b	1.0485810	1.7924989	1.7924975	0.2748645
2b+ 0.005b	1.0485836	1.7924989	1.7924985	0.2748645
2b+ 0.010b	1.0485857	1.7924989	1.7924988	0.2748645
2b+ 0.050b	1.0485877	1.7924989	1.7924988	0.2748645
2b+ 0.100b	1.0485877	1.7924989	1.7924988	0.2748645

Table 3: Variation of $[V_k^{ij}]^\infty$ with L^∞: holes case

L^∞	$\int_Y T_{22}^{11} d\boldsymbol{y}$	$\int_Y T_{12}^{12} d\boldsymbol{y}$	$\int_Y T_{11}^{22} d\boldsymbol{y}$	$\int_Y T_{22}^{22} d\boldsymbol{y}$
2b+ 0.001b	-0.0135654	0.1130969	0.0753980	-0.2005621
2b+ 0.005b	-0.0135654	0.1130969	0.0753980	-0.2005621
2b+ 0.010b	-0.0135654	0.1130969	0.0753980	-0.2005621
2b+ 0.050b	-0.0135654	0.1130969	0.0753980	-0.2005621
2b+ 0.100b	-0.0135654	0.1130969	0.0753980	-0.2005621

Table 4: Variation of $\int_Y T_{kl}^{ij} d\boldsymbol{y}$ with L^∞: holes case

4.2.2. Dependence on f

We consider two functions $f_1(y_1; a, b)$ et $f_2(y_2; a, b)$ which satisfy the condition (19) (we give their definition only for $y_1 > 0$):

	for $a \leq y_1 \leq b$
$f_1(y_1; a, b)$	$(y_1 - a)^3 (Ay_1^2 + By_1 + C)$
$f_2(y_1; a, b)$	$(y_1 - a)^3 (\alpha y_1^3 + \beta y_1^2 + \gamma y_1 + \delta)$

The comparison of $[\boldsymbol{V}^{ij,f_1}]$ with $[\boldsymbol{V}^{ij,f_2}]$ and of $\int_Y \boldsymbol{T}^{ij,f_1} d\boldsymbol{y}$ with $\int_Y \boldsymbol{T}^{ij,f_2} d\boldsymbol{y}$ confirms the independence of these coefficients from the choice of f. The values of the coefficients calculated for both f_1 and f_2 are given in the case of elastic inclusions with $p = 0$ in Tab.5 (only non-zero coefficients are given) where $a = 0.5$, $b = 4a$,$E = 1$, $E^I = 0.5$, $\nu = \nu^I = 0.25$, $R = 0.30$ and $L^\infty = 10$. The analogous situation for the holes is given in Tab.6 where : $a = 0.5$, $b = 4a$, $E = 1$, $\nu = 0.25$, $R = 0.30$ and $L^\infty = 10$.

Note that condition (19) implies that the function f is involved in the loading in problems P^{11} and P^{21}. For both problems, the influence of the function f on this loading is shown in figures (7), (8), (9) and (10).

$[V_1^{11}]^\infty$		$[V_2^{21}]^\infty$		$\int_Y T_{22}^{11}$	
f_1	f_2	f_1	f_2	f_1	f_2
0.2211406	0.2211249	0.2420602	0.2420444	-0.0010698	-0.0010739

Table 5: Result of the coefficient calculation: elastic $p = 0$ case

$[V_1^{11}]^\infty$		$[V_2^{21}]^\infty$		$\int_Y T_{22}^{11}$	
f_1	f_2	f_1	f_2	f_1	f_2
1.0485342	1.0485524	1.7922510	1.7922715	-0.0135626	-0.0136194

Table 6: Result of the coefficient calculation: holes case

4.2.3. Dependence on R

It is also interesting to study the dependence of $\left[\boldsymbol{V}^{ij}\right]^\infty$ and of $\int_Y \boldsymbol{T}^{ij} d\boldsymbol{y}$ on the radius R. In the case of holes (or equivalently of elastic inclusions with $p > 0$) the influence can be very important when the radius become almost of the same order as the period or becomes very small as one can see in Tables 7 and 8.

R	$[V_1^{11}]^\infty$	$[V_2^{12}]^\infty$	$[V_2^{21}]^\infty$	$[V_1^{22}]^\infty$
0.010	0.0008996	0.0010023	0.0010020	0.0001476
0.050	0.0226144	0.0255398	0.0255396	0.0038205
0.100	0.0918260	0.1074091	0.1074089	0.0169884
0.150	0.2124450	0.2633347	0.2633345	0.0439429
0.200	0.3949921	0.5307941	0.5307939	0.0905881
0.250	0.6601650	0.9858120	0.9858119	0.1641006
0.300	1.0486034	1.7922971	1.7922969	0.2748658
0.350	1.6469987	3.3681096	3.3681096	0.4433453
0.400	2.6773118	7.1156680	7.1156679	0.7231693
0.450	5.0071671	21.4732286	21.4732255	1.3301432
0.490	14.5258667	214.6823144	214.6821550	3.7303738

Table 7: Dependence on the radius for $\left[\boldsymbol{V}^{ij}\right]^\infty$: the hole case

R	$\int_Y T_{22}^{11} d\boldsymbol{y}$	$\int_Y T_{12}^{12} d\boldsymbol{y}$	$\int_Y T_{11}^{22} d\boldsymbol{y}$	$\int_Y T_{22}^{22} d\boldsymbol{y}$
0.010	0.0000824	0.0001257	0.0000838	-0.0005835
0.050	0.0019553	0.0031416	0.0020944	-0.0141852
0.100	0.0063660	0.0125663	0.0083775	-0.0516133
0.150	0.0097795	0.0282742	0.0188495	-0.1000315
0.200	0.0087039	0.0502653	0.0335102	-0.1464124
0.250	0.0010034	0.0785395	0.0523597	-0.1814430
0.300	-0.0135626	0.1130969	0.0753980	-0.2005602
0.350	-0.0337021	0.1539375	0.1026250	-0.2026228
0.400	-0.0574308	0.2010612	0.1340408	-0.1879331
0.450	-0.0835749	0.2544681	0.1696454	-0.1564380
0.490	-0.1054995	0.3017174	0.2011450	-0.1191938

Table 8: Dependence on the radius for $\int_Y \boldsymbol{T}^{ij} d\boldsymbol{y}$: the hole case

R	$[V_1^{11}]$	$[V_2^{12}]$	$[V_2^{21}]$	$[V_1^{22}]$
0.010	0.0002307	0.0002376	0.0002374	0.0000528
0.050	0.0057838	0.0059676	0.0059673	0.0013263
0.100	0.0232345	0.0241464	0.0241462	0.0054055
0.150	0.0526687	0.0553526	0.0553523	0.0125179
0.200	0.0946909	0.1009027	0.1009024	0.0230667
0.250	0.1503118	0.1625104	0.1625101	0.0375075
0.300	0.2211246	0.2420470	0.2420467	0.0562854
0.350	0.3113063	0.3430488	0.3430488	0.0802322
0.400	0.4220883	0.4629466	0.4629466	0.1090197
0.450	0.5613008	0.6011278	0.6011279	0.1434687
0.490	0.7019167	0.7212938	0.7212938	0.1757700

Table 9: Dependence on the radius for $\left[\boldsymbol{V}^{ij}\right]^{\infty}$: the elastic inclusion case

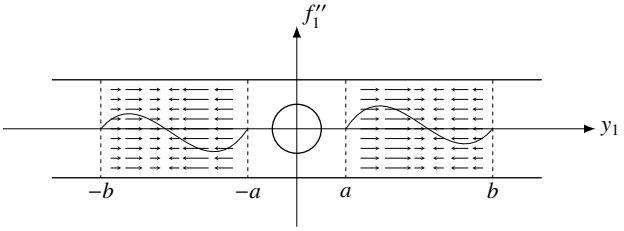

Figure 7: loading for P^{11}: $f = f_1$

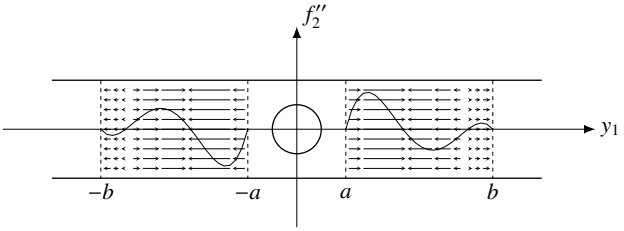

Figure 8: loading for P^{11}: $f = f_2$

For these comparisons we have chosen $a = 1.5$, $b = 3a$, $E = 1$, $\nu = 0.25$ and $L^\infty = 10$. The corresponding results obtained for elastic inclusion with $p = 0$ when $a = 1.5$, $b = 3a$, $E = 1$, $\nu = 0.25$, $E^I = 0.5$, $\nu^I = 0.25$ and $L^\infty = 10$ are given in Table 9 and Table 10.

4.2.4. Dependence on E^I/E in the case of elastic inclusions with $p = 0$

In the case of elastic inclusions with $p = 0$ it is also interesting to study the dependence of $\left[\boldsymbol{V}^{ij}\right]^\infty$ and of $\int_Y \boldsymbol{T}^{ij} d\boldsymbol{y}$ on E^I/E. We have considered the case where a=1.5, b=3*a, $R = 0.30$, E=1, $\nu = 0.25$, $\nu^I = 0.25$, $L^\infty = 10$. It is interesting to remark the difference of situations when E^I/E decreases or increases, see Tables 11, 12. When $E^I/E > 1$ (i.e. the material of the inclusion is more rigid than the surrounding material) then the coefficients $\left[\boldsymbol{V}^{ij}\right]^\infty$ become all negative and, in absolute value, monotonically increasing. In all other situations these coefficients are positive.

4.3. Validation at the macroscopic scale

The validation at the macroscopic scale should be performed by comparing $\boldsymbol{u}_0^{out} := \boldsymbol{u}^0$ and $\boldsymbol{u}_1^{out} := \boldsymbol{u}^0 + \varepsilon \boldsymbol{u}^1$ with $\boldsymbol{u}^\varepsilon$; however we can only compute $\boldsymbol{u}_h^\varepsilon$, $\boldsymbol{u}_h^0$ and $\boldsymbol{u}_h^1$. Since $\boldsymbol{u}^1$ does not belong to $\boldsymbol{H}^1(\Omega)$ but only to $\boldsymbol{Z}_0 \subset \boldsymbol{L}^2(\Omega)$ (as it has been observed in Sect. 3.2) the relative norm errors $||\boldsymbol{u}_h^\varepsilon - \boldsymbol{u}_{0,h}^{out}||/||\boldsymbol{u}_h^\varepsilon||$ and $||\boldsymbol{u}_h^\varepsilon - \boldsymbol{u}_{1,h}^{out}||/||\boldsymbol{u}_h^\varepsilon||$ are computed using the norm of $\boldsymbol{L}^2(\Omega^\varepsilon)$. The

R	$\int_Y T_{22}^{11} d\boldsymbol{y}$	$\int_Y T_{12}^{12} d\boldsymbol{y}$	$\int_Y T_{11}^{22} d\boldsymbol{y}$	$\int_Y T_{22}^{22} d\boldsymbol{y}$
0.010	0.0000053	0.0000624	0.0000416	-0.0000658
0.050	0.0001276	0.0015607	0.0010405	-0.0016190
0.100	0.0004300	0.0062428	0.0041619	-0.0061381
0.150	0.0006925	0.0140464	0.0093643	-0.0126149
0.200	0.0006464	0.0249713	0.0166476	-0.0196930
0.250	0.0000752	0.0390177	0.0260118	-0.0258496
0.300	-0.0010828	0.0564577	0.0376385	-0.0296633
0.350	-0.0025660	0.0768453	0.0512302	-0.0297693
0.400	-0.0037308	0.1003693	0.0669129	-0.0253244
0.450	-0.0033531	0.1270299	0.0846866	-0.0156543
0.490	-0.0003102	0.1506167	0.1004111	-0.0037496

Table 10: Dependence on the radius of $\int_Y \boldsymbol{T}^{ij} d\boldsymbol{y}$: the elastic inclusion case

E^I/E	$[V_1^{11}]$	$[V_2^{12}]$	$[V_2^{21}]$	$[V_1^{22}]$
0.100	0.7365879	1.0390793	1.0390789	0.1915956
0.200	0.5399045	0.6856242	0.6856239	0.1395623
0.300	0.4019328	0.4772223	0.4772220	0.1033120
0.400	0.2997924	0.3396756	0.3396752	0.0766644
0.500	0.2211262	0.2420530	0.2420527	0.0562849
0.600	0.1586740	0.1691533	0.1691530	0.0402175
0.700	0.1078900	0.1126290	0.1126287	0.0272399
0.800	0.0657828	0.0675133	0.0675130	0.0165498
0.900	0.0303030	0.0306650	0.0306647	0.0075988
1.000	-0.0000003	-0.0000000	-0.0000003	-0.0000000
2.000	-0.1624511	-0.1528339	-0.1528342	-0.0397685
3.000	-0.2285392	-0.2099850	-0.2099853	-0.0552880
4.000	-0.2643981	-0.2399011	-0.2399014	-0.0634781
5.000	-0.2869096	-0.2583075	-0.2583078	-0.0685186
6.000	-0.3023570	-0.2707759	-0.2707762	-0.0719263
7.000	-0.3136148	-0.2797811	-0.2797813	-0.0743811
8.000	-0.3221839	-0.2865902	-0.2865905	-0.0762323
9.000	-0.3289248	-0.2919194	-0.2919196	-0.0776776
10.000	-0.3343663	-0.2962038	-0.2962041	-0.0788369

Table 11: Dependence on E^I/E for $\left[\boldsymbol{V}^{ij}\right]^{\infty}$

E^I/E	$\int_Y T_{22}^{11} d\boldsymbol{y}$	$\int_Y T_{12}^{12} d\boldsymbol{y}$	$\int_Y T_{11}^{22} d\boldsymbol{y}$	$\int_Y T_{22}^{22} d\boldsymbol{y}$
0.100	-0.0079452	0.1011340	0.0674226	-0.1470031
0.200	-0.0048919	0.0898969	0.0599312	-0.1054211
0.300	-0.0030174	0.0786598	0.0524398	-0.0731051
0.400	-0.0018307	0.0674226	0.0449484	-0.0482791
0.500	-0.0010703	0.0561855	0.0374570	-0.0296238
0.600	-0.0005856	0.0449484	0.0299656	-0.0161272
0.700	-0.0002853	0.0337113	0.0224742	-0.0069946
0.800	-0.0001110	0.0224742	0.0149828	-0.0015907
0.900	-0.0000246	0.0112371	0.0074914	0.0005999
1.000	-0.0000001	-0.0000000	-0.0000000	-0.0000000
2.000	-0.0009005	-0.1123711	-0.0749141	-0.1035238
3.000	-0.0019699	-0.2247422	-0.1498281	-0.2978541
4.000	-0.0027962	-0.3371132	-0.2247422	-0.5317316
5.000	-0.0034227	-0.4494843	-0.2996562	-0.7863922
6.000	-0.0039072	-0.5618554	-0.3745703	-1.0533265
7.000	-0.0042908	-0.6742265	-0.4494843	-1.3281138
8.000	-0.0046012	-0.7865976	-0.5243984	-1.6082296
9.000	-0.0048572	-0.8989686	-0.5993124	-1.8921265
10.000	-0.0050716	-1.0113397	-0.6742265	-2.1788038

Table 12: Dependence on E^I/E for $\int_Y \boldsymbol{T}^{ij} d\boldsymbol{y}$

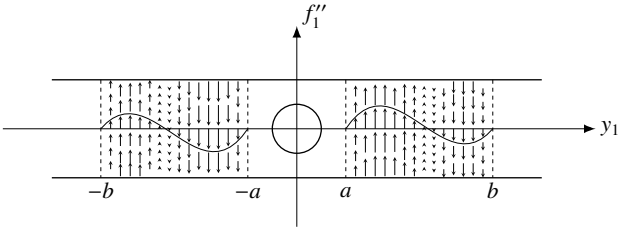

Figure 9: loading for P^{21}: $f = f_1$

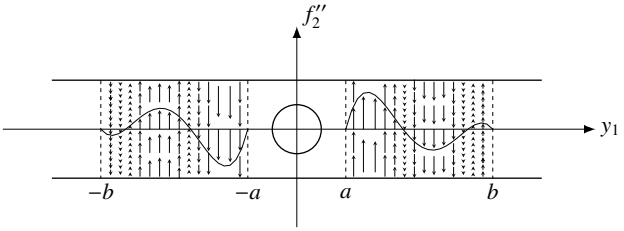

Figure 10: loading for P^{21}: $f = f_2$

numerical reference solution $\boldsymbol{u}_h^\varepsilon$ is computed on a mesh Ω_h^ε and the numerical asymptotic solutions $\boldsymbol{u}_{0,h}^{out} := \boldsymbol{u}_h^0$ and $\boldsymbol{u}_{1,h}^{out} := \boldsymbol{u}_h^0 + \varepsilon \boldsymbol{u}_h^1$ are computed on a coarse mesh Ω_h. Hence in order to compare these numerical approximations one has at first to determine by interpolation the nodal values of $\boldsymbol{u}_{0,h}^{out}$ and of $\boldsymbol{u}_{1,h}^{out}$ on Ω_h^ε. We have the following obvious estimate for $i = 0, 1$:

$$\|\boldsymbol{u}^\varepsilon - \boldsymbol{u}_i^{out}\| \leq \|\boldsymbol{u}^\varepsilon - \boldsymbol{u}_h^\varepsilon\| + \|\boldsymbol{u}_h^\varepsilon - \boldsymbol{u}_{i\ h}^{out}\| + \|\boldsymbol{u}_{i\ h}^{out} - \boldsymbol{u}_i^{out}\| \tag{48}$$

Since we compute just the term $\|\boldsymbol{u}_h^\varepsilon - \boldsymbol{u}_{i\ h}^{out}\|$ we should choose a discretization step h so that the approximation errors $\|\boldsymbol{u}^\varepsilon - \boldsymbol{u}_h^\varepsilon\|$ and $\|\boldsymbol{u}_{i\ h}^{out} - \boldsymbol{u}_i^{out}\|$ be negligible with respect to ε. This is a priori a difficult task: the abstract error estimates results on FEM approximations depend on the regularity of the solution (see [22]). For instance, since we use $P2$ finite elements, the regularity of $\boldsymbol{u}^0$ implies that for the norms in $L^2(\Omega)$ we have the estimate:

$$\|\boldsymbol{u}_{0\ h}^{out} - \boldsymbol{u}_0^{out}\| = \|\boldsymbol{u}_h^0 - \boldsymbol{u}^0\| \leq Ch^3 \tag{49}$$

However $\boldsymbol{u}^\varepsilon$ and $\boldsymbol{u}^1$ are not so regular that an analogous of (49) be valid. In any case it must be pointed out that for small values of ε it is too expensive to choose discretization steps such that the approximation errors be negligible with respect to ε. For this reasons a judicious choice of feasible and reasonable meshes is required. In most of the computations we take

a regular triangulation Ω_h of Ω with mesh-size $h = 1/120$ (and 57600 elements P2-Lagrange) and a varying mesh for Ω_h^ε where the largest mesh-size is $h_\varepsilon = 1/80$. In the case of holes, we get 32240 elements P2-Lagrange when $\varepsilon = 0.05$, 54240 when $\varepsilon = 0.025$ and 78240 when $\varepsilon = 0.0125$. In the case of elastic inclusions, we get 35440 elements P2-Lagrange when $\varepsilon = 0.05$, 59200 when $\varepsilon = 0.025$ and 88480 when $\varepsilon = 0.0125$.

The numerical results for the different situations (holes, elastic inclusions with $p = 0$ and $p = 1$) are given in tables 13, 14 and 15. It appears immediately that in all situations $||\boldsymbol{u}_h^\varepsilon - \boldsymbol{u}_{0,h}^{out}||/||\boldsymbol{u}_h^\varepsilon|| \approx \varepsilon$ and $||\boldsymbol{u}_h^\varepsilon - \boldsymbol{u}_{1,h}^{out}||/||\boldsymbol{u}_h^\varepsilon|| \approx \varepsilon^m$ with $m \gtrapprox 1.5$.

ε	$\frac{\|\|\boldsymbol{u}_h^\varepsilon - \boldsymbol{u}_{0,h}^{out}\|\|_{L^2}}{\|\|\boldsymbol{u}_h^\varepsilon\|\|_{L^2}}$	$\frac{\|\|\boldsymbol{u}_h^\varepsilon - \boldsymbol{u}_{1,h}^{out}\|\|_{L^2}}{\|\|\boldsymbol{u}_h^\varepsilon\|\|_{L^2}}$
0.05	0.0224	0.0009025
0.025	0.0112	0.0003187
0.0125	0.00559	0.0001114

Table 13: Relative errors : holes

ε	$\frac{\|\|\boldsymbol{u}_h^\varepsilon - \boldsymbol{u}_{0,h}^{out}\|\|_{L^2}}{\|\|\boldsymbol{u}_h^\varepsilon\|\|_{L^2}}$	$\frac{\|\|\boldsymbol{u}_h^\varepsilon - \boldsymbol{u}_{1,h}^{out}\|\|_{L^2}}{\|\|\boldsymbol{u}_h^\varepsilon\|\|_{L^2}}$
0.05	0.00416	0.000206
0.025	0.00206	0.0000781
0.0125	0.00101	0.0000247

Table 14: Relative errors : elastic inclusions with $p = 0$ and $E^I = 0.5E$

ε	$\frac{\|\|\boldsymbol{u}_h^\varepsilon - \boldsymbol{u}_{0,h}^{out}\|\|_{L^2}}{\|\|\boldsymbol{u}_h^\varepsilon\|\|_{L^2}}$	$\frac{\|\|\boldsymbol{u}_h^\varepsilon - \boldsymbol{u}_{1,h}^{out}\|\|_{L^2}}{\|\|\boldsymbol{u}_h^\varepsilon\|\|_{L^2}}$
0.05	0.020022435	0.001825071
0.025	0.010576063	0.000451827
0.0125	0.005423596	0.000122152

Table 15: Relative errors : elastic inclusions with $p = 1$ and $E^I = 0.5E$

Another peculiarity of the matched asymptotic expansion method is that the quality of the outer approximation increases far from the surface ω where the heterogeneities are concentrated. In order to test that $\boldsymbol{u}_{1,h}^{out}$ gives indeed a better approximation of $\boldsymbol{u}_h^\varepsilon$ far from the heterogeneities (and obviously far from the singularities of $\boldsymbol{u}_h^\varepsilon$ induced by the geometry of Ω or by the loading) we introduce for $\delta \geq 0$ the domains $\hat{\Omega}^{out}(\delta) := \{\boldsymbol{x} = (x_1, x_2) \in \Omega^\varepsilon;\ |x_1| \geq \frac{\delta}{2}\}$. We then computed the relative errors norm in $\boldsymbol{L}^2(\hat{\Omega}^{out}(\delta))$ for different values of ε in the case of the holes and in the case of elastic inclusions with $p = 0$ and $p = 1$ (see tables 16, 17 and 18).The numerical results not only agree with this property of the matched asymptotic expansion method but also prove that if one takes the same domain $\hat{\Omega}^{out}(\delta)$ then the error due to the approximation decreases with ε with an order $\gtrapprox 1.5$: see e.g. the values of $\delta/\varepsilon = 1$, resp.= 2, resp.= 4 when $\varepsilon = 0.05$, resp. $= 0.025$, resp.= 0.0125 or analogous triplet of values.

The correction of $\boldsymbol{u}^0$ by $\varepsilon\boldsymbol{u}^1$ is of order ε. One might then say that

$\varepsilon = 0.05$	
δ/ε	$\frac{\|\|\boldsymbol{u}_h^\varepsilon - \boldsymbol{u}_{1h}^{out}\|\|_{L^2}}{\|\|\boldsymbol{u}_h^\varepsilon\|\|_{L^2}}$
0.0	0.000902513
1.0	0.000841890
1.2	0.000837274
1.4	0.000834825
1.6	0.000833395
1.8	0.000832471
2.0	0.000831834
3.0	0.000830932

$\varepsilon = 0.025$	
δ/ε	$\frac{\|\|\boldsymbol{u}_h^\varepsilon - \boldsymbol{u}_{1h}^{out}\|\|_{L^2}}{\|\|\boldsymbol{u}_h^\varepsilon\|\|_{L^2}}$
0.0	0.000318681
2.0	0.000296530
3.0	0.000295194
4.0	0.000294175
5.0	0.000293475
6.0	0.000293108
7.0	0.000292848
8.0	0.000292778

$\varepsilon = 0.0125$	
δ/ε	$\frac{\|\|\boldsymbol{u}_h^\varepsilon - \boldsymbol{u}_{1h}^{out}\|\|_{L^2}}{\|\|\boldsymbol{u}_h^\varepsilon\|\|_{L^2}}$
0.0	0.000111381
2.0	0.000106239
4.0	0.000104731
6.0	0.000103745
8.0	0.000102848
10.0	0.000102221
12.0	0.000101790
16.0	0.000101313
20.0	0.000101085

Table 16: Evolution of the exterior approximation in $\hat{\Omega}^{out}(\delta)$: holes

the need to calculate $\boldsymbol{u}^1$ depends on the precision with which one wishes to estimate $\boldsymbol{u}^\varepsilon$. However it is important to remember that $\boldsymbol{u}_0^{out}$ and $\boldsymbol{u}_1^{out}$ do not provide any information about inclusions and the approximation of the behaviour of $\boldsymbol{u}^\varepsilon$ in the layer $\Omega^{in,\varepsilon}$ by the inner term $\boldsymbol{v}^0 + \varepsilon\boldsymbol{v}^1$ requires the calculation of $\boldsymbol{u}^1$ to recover the uniqueness of $\boldsymbol{v}^1$ (see remark 2.2.1). Therefore the implementation and validation of the computation of $\boldsymbol{u}_h^1$ is necessary.

$\varepsilon = 0.05$	
δ/ε	$\frac{\|\|\boldsymbol{u}_h^\varepsilon - \boldsymbol{u}_{1h}^{out}\|\|_{L^2}}{\|\|\boldsymbol{u}_h^\varepsilon\|\|_{L^2}}$
0.0	0.000205545
1.0	0.000189485
1.2	0.000189295
1.4	0.000188847
1.6	0.000188449
1.8	0.000188183
2.0	0.000187997
3.0	0.000187725
4.0	0.000187797

$\varepsilon = 0.025$	
δ/ε	$\frac{\|\|\boldsymbol{u}_h^\varepsilon - \boldsymbol{u}_{1h}^{out}\|\|_{L^2}}{\|\|\boldsymbol{u}_h^\varepsilon\|\|_{L^2}}$
0.0	0.000078085
1.0	0.000072545
2.0	0.000071793
3.0	0.000071304
4.0	0.000070938
5.0	0.000070701
6.0	0.000070564
7.0	0.000070465
8.0	0.000070419
9.0	0.000070414
10.0	0.000070431

$\varepsilon = 0.0125$	
δ/ε	$\frac{\|\|\boldsymbol{u}_h^\varepsilon - \boldsymbol{u}_{1h}^{out}\|\|_{L^2}}{\|\|\boldsymbol{u}_h^\varepsilon\|\|_{L^2}}$
0.0	0.000024692
2.0	0.000021741
4.0	0.000021028
6.0	0.000020559
8.0	0.000020086
10.0	0.000019666
12.0	0.000019367
14.0	0.000019129
16.0	0.000018938
20.0	0.000018588

Table 17: Evolution of the exterior approximation in $\hat{\Omega}^{out}(\delta)$: elastic inclusions $p = 0$, $E^I = 0.5E$

$\varepsilon = 0.05$	
δ/ε	$\frac{\|\|\boldsymbol{u}_h^\varepsilon - \boldsymbol{u}_{1h}^{out}\|\|_{L^2}}{\|\|\boldsymbol{u}_h^\varepsilon\|\|_{L^2}}$
0.0	0.001825071
1.0	0.001759737
1.2	0.001757144
1.4	0.001755302
1.6	0.001753779
1.8	0.001752386
2.0	0.001751041
3.0	0.001747021
4.0	0.001741251
5.0	0.001736350

$\varepsilon = 0.025$	
δ/ε	$\frac{\|\|\boldsymbol{u}_h^\varepsilon - \boldsymbol{u}_{1h}^{out}\|\|_{L^2}}{\|\|\boldsymbol{u}_h^\varepsilon\|\|_{L^2}}$
0.0	0.000451827
1.0	0.000422243
2.0	0.000417829
3.0	0.000415797
4.0	0.000413844
5.0	0.000412015
6.0	0.000410613
7.0	0.000408883
8.0	0.000407363
10.0	0.000404803

$\varepsilon = 0.0125$	
δ/ε	$\frac{\|\|\boldsymbol{u}_h^\varepsilon - \boldsymbol{u}_{1h}^{out}\|\|_{L^2}}{\|\|\boldsymbol{u}_h^\varepsilon\|\|_{L^2}}$
0.0	0.000122152
2.0	0.000109975
4.0	0.000108002
6.0	0.000106582
8.0	0.000105119
10.0	0.000103909
12.0	0.000102889
14.0	0.000101912
16.0	0.000101275
20.0	0.000099688

Table 18: Evolution of the exterior approximation in $\hat{\Omega}^{out}(\delta)$: elastic inclusions $p = 1$ and $E^I = 0.5E$

$\varepsilon = 0.05$	
η/ε	$\frac{\|\|\boldsymbol{u}_h^\varepsilon - \boldsymbol{u}_{1h}^{inn}\|\|_{L^2}}{\|\|\boldsymbol{u}_h^\varepsilon\|\|_{L^2}}$
1.2	0.002774
1.4	0.002751
1.6	0.002780

$\varepsilon = 0.025$	
η/ε	$\frac{\|\|\boldsymbol{u}_h^\varepsilon - \boldsymbol{u}_{1h}^{inn}\|\|_{L^2}}{\|\|\boldsymbol{u}_h^\varepsilon\|\|_{L^2}}$
1.2	0.001036958
1.4	0.001005650
1.6	0.001000810
1.8	0.001002316
2.0	0.001016178

$\varepsilon = 0.0125$	
η/ε	$\frac{\|\|\boldsymbol{u}_h^\varepsilon - \boldsymbol{u}_{1h}^{inn}\|\|_{L^2}}{\|\|\boldsymbol{u}_h^\varepsilon\|\|_{L^2}}$
1.2	0.000414496
1.4	0.000408768
1.6	0.000400531
1.8	0.000394518
2.0	0.000391273
2.2	0.000404875
2.4	0.000408182

Table 19: Evolution of the interior approximation in $\Omega^{\eta,\varepsilon}$: holes

4.4. Validation at the microscopic scale

Let us remark at first that as shown in (16) $\boldsymbol{u}_{0,h}^{inn} := \boldsymbol{u}_h^0$ is independent from the inclusions. Hence this validation will be realized studying the relative error norms for $\boldsymbol{u}_{1,h}^{inn}$ in a suitably defined domain $\Omega_h^{in}(\varepsilon)$ whose thickness is given by the function $\eta(\varepsilon)$ which is not explicitly defined. As has been previously remarked at the beginning of sect. 4.3, in order to compute these relative error norms one must determine the nodal values of $\boldsymbol{u}_{1,h}^{inn} := \boldsymbol{v}_h^0 + \varepsilon \boldsymbol{v}_h^1$ on the mesh Ω_h^ε where the numerical reference solution $\boldsymbol{u}_h^\varepsilon$ is defined. We use the same meshes as for the macroscopic scale validation. In order to evaluate $\eta(\varepsilon)$ at first we compute for increasing values of $\eta > 0$ the relative errors $\frac{||\boldsymbol{u}_h^\varepsilon - \boldsymbol{u}_{1h}^{inn}||_{L^2}}{||\boldsymbol{u}_h^\varepsilon||_{L^2}}$ in the domain $\Omega^{\eta,\varepsilon} = \{\boldsymbol{x} = (x_1, x_2) \in \Omega^\varepsilon : |x_1| < \frac{\eta}{2}\}$. Then $\eta(\varepsilon)$ will be in the interval between the value of η such that this relative errors is minimum and the next value of η. In the case of holes the results are given in table 19. We also give in table 20 the estimated value of $\eta(\varepsilon)$ and of $\eta(\varepsilon)/\varepsilon$. For elastic inclusions with $p = 0$ and $E^I = 0.5E$ the analogous results are given in tables 21 and 22. All these results are in agreement with the asymptotic assumptions, in particular with (3).

$\varepsilon = 0.05$	$0.07 \leq \eta(\varepsilon) \leq 0.08$	$1.4 \leq \eta(\varepsilon)/\varepsilon \leq 1.6$
$\varepsilon = 0.025$	$0.04 \leq \eta(\varepsilon) \leq 0.045$	$1.6 \leq \eta(\varepsilon)/\varepsilon \leq 1.8$
$\varepsilon = 0.0125$	$0.025 \leq \eta(\varepsilon) \leq 0.0275$	$2 \leq \eta(\varepsilon)/\varepsilon \leq 2.2$

Table 20: Evolution of $\eta(\varepsilon)$ and of $\eta(\varepsilon)/\varepsilon$ with ε: holes

$\varepsilon = 0.05$	
η/ε	$\frac{\|\|\boldsymbol{u}_h^\varepsilon - \boldsymbol{u}_{1h}^{inn}\|\|_{L^2}}{\|\|\boldsymbol{u}_h^\varepsilon\|\|_{L^2}}$
1.0	0.0006462
1.2	0.0006605
1.4	0.0006968

$\varepsilon = 0.025$	
η/ε	$\frac{\|\|\boldsymbol{u}_h^\varepsilon - \boldsymbol{u}_{1h}^{inn}\|\|_{L^2}}{\|\|\boldsymbol{u}_h^\varepsilon\|\|_{L^2}}$
1.0	0.0002882
1.2	0.0002837
1.4	0.0002848
1.6	0.0002917

$\varepsilon = 0.0125$	
η/ε	$\frac{\|\|\boldsymbol{u}_h^\varepsilon - \boldsymbol{u}_{1h}^{inn}\|\|_{L^2}}{\|\|\boldsymbol{u}_h^\varepsilon\|\|_{L^2}}$
1.2	0.0001341
1.4	0.0001330
1.6	0.0001312
1.8	0.0001299
2.0	0.0001302

Table 21: Evolution of the interior approximation in $\Omega^{\eta,\varepsilon}$; elastic inclusions: $p = 0$, $E^I = 0.5E$

$\varepsilon = 0.05$	$0.05 \leq \eta(\varepsilon) \leq 0.06$	$1. \leq \eta(\varepsilon)/\varepsilon \leq 1.2$
$\varepsilon = 0.025$	$0.03 \leq \eta(\varepsilon) \leq 0.035$	$1.2 \leq \eta(\varepsilon)/\varepsilon \leq 1.4$
$\varepsilon = 0.0125$	$0.0225 \leq \eta(\varepsilon) \leq 0.025$	$1.8 \leq \eta(\varepsilon)/\varepsilon \leq 2.$

Table 22: Evolution of $\eta(\varepsilon)$ and of $\eta(\varepsilon)/\varepsilon$ with ε; elastic inclusions: $p = 0$, $E^I = 0.5E$

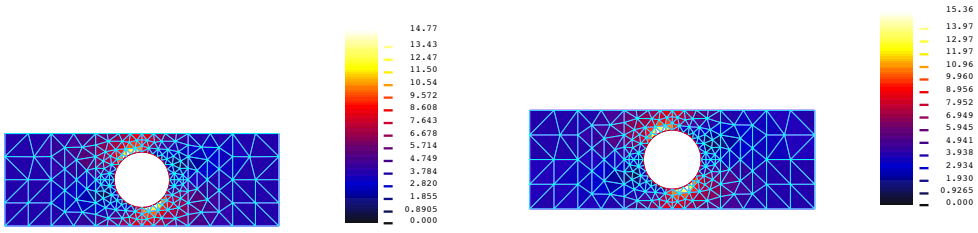

Figure 11: Comparison of $\boldsymbol{\sigma}_h^{\varepsilon,VM}$ (left) and $\boldsymbol{\tau}_h^{0,VM}$ (right) in $\mathcal{U}_1^\varepsilon$

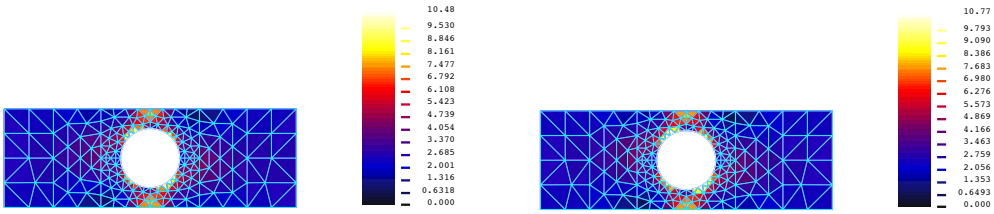

Figure 12: Comparison of $\boldsymbol{\sigma}_h^{\varepsilon,VM}$ (left) and $\boldsymbol{\tau}_h^{0,VM}$ (right) in $\mathcal{U}_2^\varepsilon$

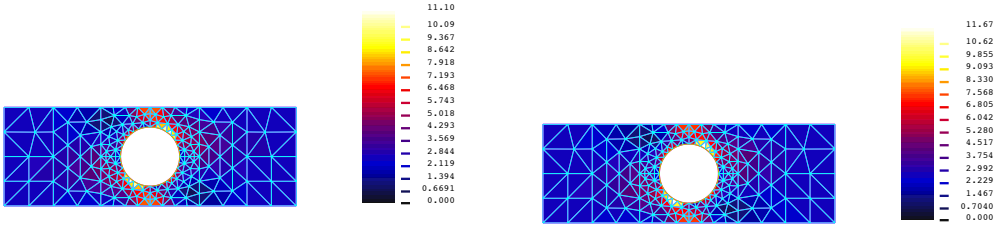

Figure 13: Comparaison of $\boldsymbol{\sigma}_h^{\varepsilon,VM}$ (left) and $\boldsymbol{\tau}_h^{0,VM}$ (right) in $\mathcal{U}_3^\varepsilon$

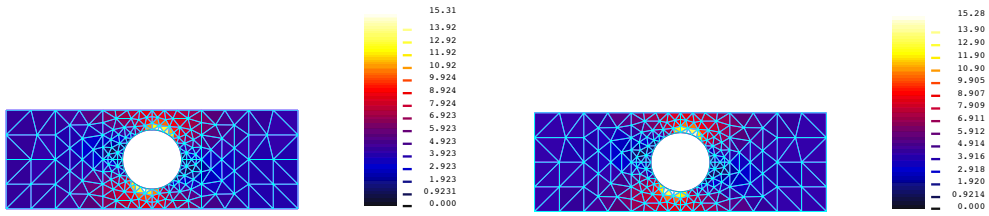

Figure 14: Comparaison of $\boldsymbol{\sigma}_h^{\varepsilon,VM}$ (left) and $\boldsymbol{\tau}_h^{0,VM}$ (right) in $\mathcal{U}_4^\varepsilon$

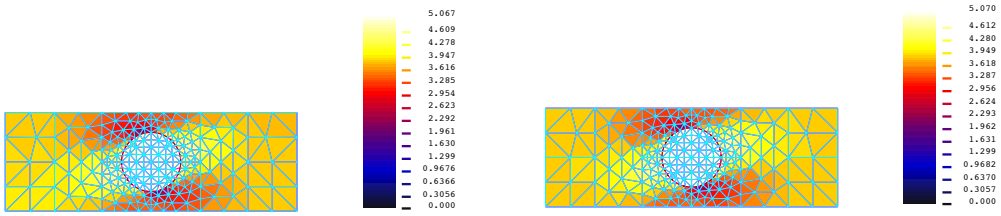

Figure 15: Comparison of $\boldsymbol{\sigma}_h^{\varepsilon,VM}$ (left) and $\boldsymbol{\tau}_h^{0,VM}$ (right) in $\mathcal{U}_1^\varepsilon$, elastic inclusion with $E^I/E = 4$

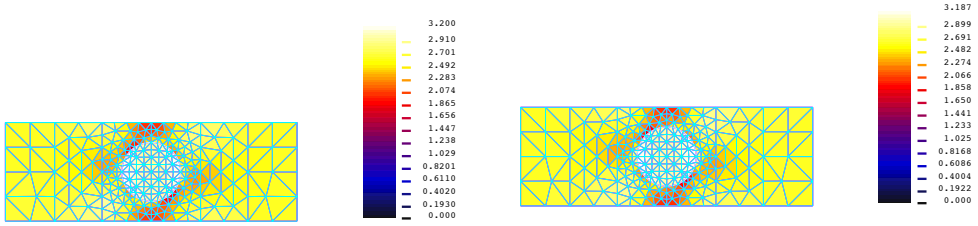

Figure 16: Comparison of $\boldsymbol{\sigma}_h^{\varepsilon,VM}$ (left) and $\boldsymbol{\tau}_h^{0,VM}$ (right) in $\mathcal{U}_2^\varepsilon$, elastic inclusion with $E^I/E = 4$

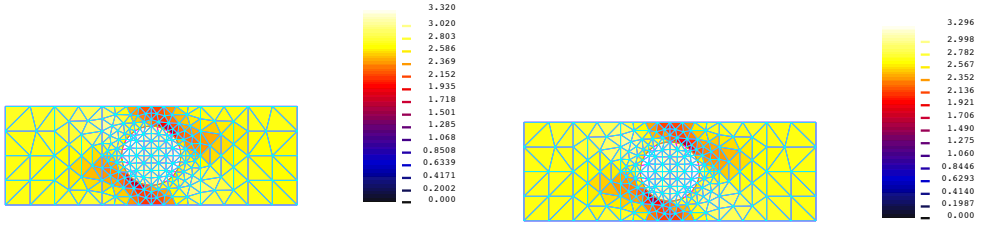

Figure 17: Comparaison of $\boldsymbol{\sigma}_h^{\varepsilon,VM}$ (left) and $\boldsymbol{\tau}_h^{0,VM}$ (right) in $\mathcal{U}_3^\varepsilon$, elastic inclusion with $E^I/E = 4$

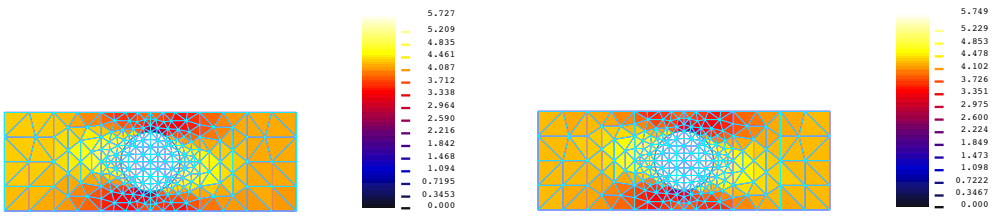

Figure 18: Comparison of $\boldsymbol{\sigma}_h^{\varepsilon,VM}$ (left) and $\boldsymbol{\tau}_h^{0,VM}$ (right) in $\mathcal{U}_4^\varepsilon$, elastic inclusion with $E^I/E = 4$

Important informations on the behaviour of the structure are given by the stress field, in particular near the inclusions. In order to validate our asymptotic model it is therefore important to compare $\boldsymbol{\sigma}_h^\varepsilon$ and $\boldsymbol{\tau_h}^0$ near the inclusions. In the following this comparison is done for $\varepsilon = 0.0125$, for both holes and elastic inclusions with $p = 0$. We consider 4 inclusions $\mathcal{I}_k^\varepsilon$, $k = 1, 2, 3$ and 4, located in Ω^ε by their center of coordinates $(x_1 = 0, x_2^k)$ with $x_2^k = -20\varepsilon$, $-\varepsilon$, 10ε and 30ε. Let $\boldsymbol{\sigma}_h^{\varepsilon,VM}$ (resp. $\boldsymbol{\tau}_h^{0,VM}$), denote the equivalent Von Mises stress of $\boldsymbol{\sigma}_h^\varepsilon$ (resp. $\boldsymbol{\tau_h}^0$). We plot the isovalues of $\boldsymbol{\sigma}_h^{\varepsilon,VM}$ in a suitable neighbourhood $\mathcal{U}_k^\varepsilon$ of each inclusion and we compare them to the isovalues of $\boldsymbol{\tau}_h^{0,VM}$. The results in the case of holes are given in fig. 11, 12, 13 and 14; in the case of elastic inclusions with $p = 0$ and $E^I/E = 4$ in fig.15, 16, 17 and 18.

5. Concluding remarks

The numerical algorithm which combines matched asymptotic expansions and domain decomposition is an efficient tool to effectively solve multi-scale problems with a large number of heterogeneities. The zero order problems do not consider the heterogeneities and hence give no information on the microscopic behaviour near the heterogeneities. However the first order problems allow to obtain the necessary informations in order to reconstruct displacement and stress fields around the heterogeneities.

As in the classical homogenization [3], [4], [5], [6] the coefficients useful for the first order problems can be easily computed once for all as solutions

of cell problems. Indeed these cell problems do not depend on the forces and displacements imposed on the whole structure, but only on the geometry of the heterogeneities and on the material properties. Many computations have been done in order to stress the dependence of these coefficients on the geometric and materials parameters: for instance the diameter in the case of the holes and the relative strength for elastic inclusions.

The zeroth and the first order approximations are computed on a structure without the heterogeneities using a coarse mesh simple to obtain. The numerical validation proves that the informations so obtained are as good as the informations obtained on the real structure on a very fine and difficult to realize mesh.

At last let us emphasize that the numerical experiments agree with the assumptions of the ansatz at the basis of the matched asymptotic expansion method.

Appendix

In order to avoid inessential technicalities we consider the following simplified form of the first order problem (32) where we assume that ω is at least of class $\mathcal{C}^2$, that $\omega \cap \partial\Omega = \emptyset$ and that $\partial\Omega_u = \partial\Omega$:

$$\left\{\begin{array}{lcll} -\boldsymbol{div}\boldsymbol{\sigma}(\boldsymbol{u}) & = & \boldsymbol{f} & \text{in } \Omega \\ \boldsymbol{\sigma}(\boldsymbol{u}) & = & \boldsymbol{A}\boldsymbol{\gamma}(\boldsymbol{u}) & \text{in } \Omega \\ \boldsymbol{u} & = & 0 & \text{on } \partial\Omega \\ [\boldsymbol{u}] & = & \boldsymbol{g} & \text{on } \omega \\ [\boldsymbol{\sigma}(\boldsymbol{u})\boldsymbol{n}] & = & \boldsymbol{h} & \text{on } \omega \end{array}\right. \tag{50}$$

where $\boldsymbol{f} \in \boldsymbol{L}^2(\Omega)$, $\boldsymbol{g} \in \boldsymbol{H}^{-1/2}(\omega)$ and $\boldsymbol{h} \in \boldsymbol{H}^{-3/2}(\omega)$ denote the gap in displacements and in normal stresses on ω. These data are known and can be computed once the zero order problem is solved. Let us remark at first that the solution $\boldsymbol{u}$ of (43) does not belong to $\boldsymbol{H}^1(\Omega)$. More precisely, let be $\Omega_1 := \Omega^+$, $\Omega_2 := \Omega^-$ and :

$$\boldsymbol{Z} := \{\boldsymbol{z} \in \boldsymbol{L}^2(\Omega); \mathbf{div}(\boldsymbol{A}\boldsymbol{\gamma}(\boldsymbol{z}|_{\Omega_i}) \in \boldsymbol{L}^2(\Omega_i)\}; \tag{51}$$

equipped with the natural graph norm. Then $\boldsymbol{u} \in \boldsymbol{Z}$. Since $(\boldsymbol{z}|_{\Omega_i})|_\omega$ and $((\boldsymbol{A}\boldsymbol{\gamma}(\boldsymbol{z}|_{\Omega_i})\boldsymbol{n})|_\omega$ cannot have a classical meaning for $\boldsymbol{u} \in \boldsymbol{Z}$ the transmission conditions $[\boldsymbol{u}] = \boldsymbol{\mathcal{G}_d}$ and $[\boldsymbol{\sigma}(\boldsymbol{u})\boldsymbol{n}] = \boldsymbol{\mathcal{G}_{nS}}$ on ω have to be taken in a weak sense adapting the methods of Lions-Magenes [20]. Let us consider separately

Ω_1 and Ω_2 and with an obvious notation $\boldsymbol{Z}(\Omega_i)$ and let us assume that the elasticity tensor $\mathbf{A}$ is constant on each Ω_i. We drop the index i since the reasoning is the same for both cases. As in distribution theory $\boldsymbol{z}|_\omega$ and $(\boldsymbol{A}\boldsymbol{\gamma}(\boldsymbol{z})\boldsymbol{n})|_\omega$ will be defined by duality.

Theorem 1. *The space* $\mathcal{C}^\infty(\bar{\Omega};\mathbf{R}^3)$ *is dense in* $\boldsymbol{Z}(\Omega)$.

Proof. Let be $\mathbf{u} \longrightarrow \mathbf{L}(\mathbf{u})$ a linear and continuous form on $\boldsymbol{Z}(\Omega)$; since $\boldsymbol{L}^2(\Omega)$ is an Hilbert space there exist $\Psi, \Phi \in \boldsymbol{L}^2(\Omega)$ such that:

$$\mathbf{L}(\mathbf{u}) = \int_\Omega \Psi\mathbf{u}dx + \int_\Omega \Phi\mathbf{div}\boldsymbol{A}\boldsymbol{\gamma}(\boldsymbol{u})dx \tag{52}$$

To conclude it is enough to prove that if

$$\mathbf{L}(\theta) = 0 \quad \text{for all} \quad \theta \in \mathcal{C}^\infty(\bar{\Omega};\mathbf{R}^3) \tag{53}$$

then $\mathbf{L}(\mathbf{u}) = 0$ for all $\mathbf{u} \in \boldsymbol{Z}(\Omega)$. Since every $\theta \in \mathcal{C}^\infty(\bar{\Omega};\mathbf{R}^3)$ is the restriction to Ω of (at least) one $\Theta \in \mathcal{D}(\mathbf{R}^3;\mathbf{R}^3)$ then we can write (53) a s:

$$\mathbf{L}(\theta) = \int_{\mathbf{R}^3} \tilde{\Psi}\Theta dx + \int_{\mathbf{R}^3} \tilde{\Phi}\mathbf{div}\boldsymbol{A}\boldsymbol{\gamma}(\Theta)dx = 0 \tag{54}$$

where $\tilde{\Psi}, \tilde{\Phi} \in \boldsymbol{L}^2(\mathbf{R}^3)$ are the extensions with 0 outside Ω of $\Psi, \Phi \in \boldsymbol{L}^2(\Omega)$. Equation (54) means that in the distributions sense on $\mathbf{R}^3$ one has

$$\mathbf{div}\boldsymbol{A}\boldsymbol{\gamma}(\tilde{\Phi}) = -\tilde{\Psi} \tag{55}$$

and hence (local regularity of elliptic systems) that $\tilde{\Phi} \in \boldsymbol{H}^2(\tilde{\Omega})$ for any bounded $\tilde{\Omega} \supset \bar{\Omega}$. This means that indeed $\Phi \in \boldsymbol{H}_0^2(\Omega)$ and so integrating by parts (52) we get thanks to (54) $\mathbf{L}(\mathbf{u}) = \int_\Omega (\mathbf{div}\boldsymbol{A}\boldsymbol{\gamma}(\Phi) + \Psi)\mathbf{u}dx = 0$. ∎

Before to state and prove the fundamental result we recall the following lemma.

Lemma 1. *The map* $\mathfrak{tr} := \mathbf{v} \longrightarrow (\mathbf{v}|_\omega, (\boldsymbol{A}\boldsymbol{\gamma}(\boldsymbol{v})\boldsymbol{n})|_\omega)$ *is linear, continuous and onto from* $\boldsymbol{H}^2(\Omega)$ *onto* $\boldsymbol{H}^{3/2}(\omega) \times \boldsymbol{H}^{1/2}(\omega)$ *and admits a non-unique linear right-inverse* $\mathfrak{R}$*; moreover ker*$(\mathfrak{tr}) = \boldsymbol{H}_0^2(\Omega)$

The lemma is a particular case of a more general result on the so-called Cauchy data proved by Grubb, see e.g. [23] and the bibliography therein.

Theorem 2. *The trace map* $\mathfrak{tr} : \mathbf{u} \longrightarrow \mathfrak{tr}(\mathbf{u}) := (\mathbf{u}|_\omega, (\boldsymbol{A\gamma}(\boldsymbol{u})\boldsymbol{n})|_\omega)$ *defined on* $\mathcal{C}^\infty(\bar{\Omega}; \mathbf{R}^3)$ *can be extended by continuity to a linear and continuous map, denoted* $\mathfrak{TR}$*, from* $\boldsymbol{Z}(\Omega)$ *into* $\boldsymbol{H}^{-1/2}(\omega) \times \boldsymbol{H}^{-3/2}(\omega)$.

Proof. Let be given $(\eta, \varrho) \in \boldsymbol{H}^{3/2}(\omega) \times \boldsymbol{H}^{1/2}(\omega)$ and let be $\mathbf{v}(\eta, \varrho) := \mathfrak{R}(-\eta, \varrho)$ where $\mathfrak{R}$ is one linear right inverse. Let now define on $\boldsymbol{Z}(\Omega) \times (\boldsymbol{H}^{3/2}(\omega) \times \boldsymbol{H}^{1/2}(\omega))$ the bilinear and bi-continuous form:

$$L(\mathbf{u}, (\eta, \varrho)) = \int_\Omega \mathbf{u}\mathbf{div}\boldsymbol{A\gamma}(\mathbf{v})dx - \int_\Omega \mathbf{div}\boldsymbol{A\gamma}(\mathbf{u})\mathbf{v}dx \tag{56}$$

Let us at first remark that $L(\mathbf{u}, (\eta, \varrho))$ is well defined since it does not depend on the particular right inverse $\mathfrak{R}$ chosen. Indeed if $\mathbf{v}(\eta, \varrho)$ and $\mathbf{v}_1(\eta, \varrho)$ correspond to two different right inverses then $(\mathbf{v}(\eta, \varrho) - \mathbf{v}_1(\eta, \varrho)) \in \boldsymbol{H}_0^2(\Omega)$. The density of $\mathcal{D}(\mathbf{R}^3; \mathbf{R}^3)$ in $\boldsymbol{H}_0^2(\Omega)$ and (56) imply the result. It is also obvious that $L(\mathbf{u}, (\eta, \varrho))$ is bi-continuous and hence there exists a linear and continuous map $\mathfrak{TR}$, from $\boldsymbol{Z}(\Omega)$ to $\boldsymbol{H}^{-1/2}(\omega) \times \boldsymbol{H}^{-3/2}(\omega)$ such that

$$L(\mathbf{u}, (\eta, \varrho)) =< \mathfrak{TR}\mathbf{u}, (\eta, \varrho) > \tag{57}$$

where $< \bullet, \bullet >$ denotes the duality between $\boldsymbol{H}^{-1/2}(\omega) \times \boldsymbol{H}^{-3/2}(\omega)$ and $\boldsymbol{H}^{1/2}(\omega) \times \boldsymbol{H}^{3/2}(\omega)$. When $\mathbf{u} \in \mathcal{C}^\infty(\bar{\Omega}; \mathbf{R}^3)$ then the Green formula, (56) and (57) imply that $\mathfrak{TR}\mathbf{u} = (\mathbf{u}|_\omega, (\boldsymbol{A\gamma}(\boldsymbol{u})\boldsymbol{n})|_\omega)$. Hence Theorem 1 implies the result. ∎

Remark 1: Let us explicitly remark that the generic form of the first order problem (32) implies that $\mathbf{u} \in \boldsymbol{Z}_0 := \{\boldsymbol{z} \in \boldsymbol{L}^2(\Omega); \mathbf{div}(\boldsymbol{A\gamma}(\boldsymbol{z}|_{\Omega_i}) = 0)\}$; .

[1] G. Geymonat, S. Hendili, F. Krasucki, M. Vidrascu, The matched asymptotic expansion for the computation of the effective behavior of an elastic structure with a thin layer of holes, International Journal for Multiscale Computational Engineering 9 (5) (2011) 529–542. doi:10.1615/IntJMultCompEng.v9.i5.
URL `http://hal.inria.fr/inria-00540992`

[2] G. Geymonat, S. Hendili, F. Krasucki, M. Vidrascu, Matched asymptotic expansion method for an homogenized interface model., accepted for pub M3AS approximately on issue 03(24)2014 (Nov. 2014).
URL `http://hal.archives-ouvertes.fr/hal-00757005`

[3] A. Bensoussan, J.-L. Lions, G. Papanicolaou, Asymptotic analysis for periodic structures, AMS Chelsea Publishing, Providence, RI, 2011, corrected reprint of the 1978 original [MR0503330].

[4] O. A. Oleinik, A. S. Shamaev, G. A. Yosifian, Mathematical problems in elasticity and homogenization, Vol. 26 of Studies in Mathematics and its Applications, North-Holland Publishing Co., Amsterdam, 1992.

[5] D. Cioranescu, P. Donato, An introduction to homogenization, Vol. 17 of Oxford Lecture Series in Mathematics and its Applications, The Clarendon Press Oxford University Press, New York, 1999.

[6] E. Sánchez-Palencia, Nonhomogeneous media and vibration theory, Vol. 127 of Lecture Notes in Physics, Springer-Verlag, Berlin, 1980.

[7] A.-L. Bessoud, F. Krasucki, G. Michaille, Multi-materials with strong interface: Variational modelings, Asymptotic Analysis 61 (2009) 1–19. doi:10.3233/ASY-2008-0903.
URL http://hal.archives-ouvertes.fr/hal-00790347

[8] G. Geymonat, S. Hendili, F. Krasucki, M. Serpilli, M. Vidrascu, Asymptotic expansions and domain decomposition, in: 21st International Conference on Domain Decomposition Methods, Rennes, France, 2013.
URL http://hal.inria.fr/hal-00794531

[9] G. Geymonat, F. Krasucki, D. Marini, M. Vidrascu, A domain decomposition method for a bonded structure, Math. Models Methods Appl. Sci. 8 (8) (1998) 1387–1402. doi:10.1142/S0218202598000652.
URL http://dx.doi.org/10.1142/S0218202598000652

[10] N. Nguetseng, E. Sánchez-Palencia, Stress concentration for defects distributed near a surface, in: Local effects in the analysis of structures (Cachan, 1984), Vol. 12 of Stud. Appl. Mech., Elsevier, Amsterdam, 1985, pp. 55–74.

[11] E. Sánchez-Palencia, Elastic body with defects distributed near a surface, in: Homogenization Techniques for Composite Media, Springer, 1987, pp. 183–192.

[12] R. Abdelmoula, A. Leger, Local and global effects of small holes periodically distributed on a surface embedded in an axisymmetrical elastic medium, Eur. J. Mech. A Solids 24 (1) (2005) 89–109. doi:10.1016/j.euromechsol.2004.10.004.
URL http://dx.doi.org/10.1016/j.euromechsol.2004.10.004

[13] R. Abdelmoula, J.-J. Marigo, The effective behavior of a fiber bridged crack, J. Mech. Phys. Solids 48 (11) (2000) 2419–2444. doi:10.1016/S0022-5096(00)00003-X.
URL http://dx.doi.org/10.1016/S0022-5096(00)00003-X

[14] M. David, C. Pideri, J.-J. Marigo, Homogenized Interface Model Describing Inhomogeneities Located on a Surface, Journal of Elasticity (2011) accepté le 8/12/2011doi:10.1007/s10659-012-9382-5.
URL http://hal.archives-ouvertes.fr/hal-00655496

[15] J.-J. Marigo, C. Pideri, The effective behavior of elastic bodies containing microcracks or microholes localized on a surface, International Journal of Damage Mechanics 20 (Special issue of ESMC2009) (2011) pages 1151–1177. doi:10.1177/1056789511406914.
URL http://hal-polytechnique.archives-ouvertes.fr/hal-00549546

[16] P. Le Tallec, Domain decomposition methods in computational mechanics, in: J. T. Oden (Ed.), Computational Mechanics Advances, Vol. 1 (2), North-Holland, 1994, pp. 121–220.

[17] E.-X. Roux, Acceleration of the outer conjugate gradient by reorthogonalization for a domain decomposition method with lagrange multiplier, in: Proc. Third Intnl. Symp. Domain Decomposition methods, SIAM, 1990, pp. 314–321.

[18] P. Le Tallec, M. Vidrascu, Solving Large Scale Structural Problems on Parallel Computers using Domain Decomposition Techniques, m. papadrakakis Edition, J. Wiley, 1996, Ch. 3, pp. 49–82.

[19] C. Farhat, F.-X. Roux, Implicit parallel processing in structural mechanics, Comput. Mech. Adv. 2 (1) (1994) 124.

[20] J.-L. Lions, E. Magenes, Problèmes aux limites non homogènes et applications. Vol. 1, Travaux et Recherches Mathématiques, No. 17, Dunod, Paris, 1968.

[21] A. Ralston, A first course in numerical analysis, McGraw-Hill Book Co., New York, 1965.

[22] P. G. Ciarlet, The finite element method for elliptic problems, Vol. 40 of Classics in Applied Mathematics, Society for Industrial and Applied Mathematics (SIAM), Philadelphia, PA, 2002, reprint of the 1978 original [North-Holland, Amsterdam; MR0520174 (58 #25001)]. doi:10.1137/1.9780898719208.
URL http://dx.doi.org/10.1137/1.9780898719208

[23] G. Grubb, Distributions and operators, Vol. 252 of Graduate Texts in Mathematics, Springer, New York, 2009.